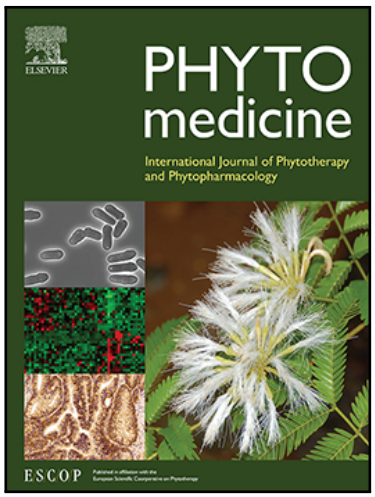

Khellin as a selective monoamine oxidase B inhibitor ameliorated paclitaxel-induced peripheral neuropathy in mice

Xingnan Ouyang , Danyang Zhu , Yujie Huang , Xuejian Zhao , Rui Xu , Jiaying Wang , Wenjun Li , Xu Shen

PII: S0944-7113(23)00033-8
DOI: https://doi.org/10.1016/j.phymed.2023.154673
Reference: PHYMED 154673

To appear in: *Phytomedicine*

Received date: 18 October 2022
Revised date: 28 December 2022
Accepted date: 12 January 2023

Please cite this article as: Xingnan Ouyang , Danyang Zhu , Yujie Huang , Xuejian Zhao , Rui Xu , Jiaying Wang , Wenjun Li , Xu Shen , Khellin as a selective monoamine oxidase B inhibitor ameliorated paclitaxel-induced peripheral neuropathy in mice, *Phytomedicine* (2023), doi: https://doi.org/10.1016/j.phymed.2023.154673

Original Article

Khellin as a selective monoamine oxidase B inhibitor ameliorated paclitaxel-induced peripheral neuropathy in mice

Xingnan Ouyang[1, 3≠], Danyang Zhu[1≠], Yujie Huang[1], Xuejian Zhao[1], Rui Xu[1], Jiaying Wang[1*], Wenjun Li[1*] and Xu Shen[1, 2*]

[1]Jiangsu Key Laboratory of Drug Target and Drug for Degenerative Diseases, School of Medicine& Holistic Integrative Medicine, Nanjing University of Chinese Medicine, Nanjing 210023, China.

[2]National Key Laboratory on Technologies for Chinese Medicine Pharmaceutical Process Control and Intelligent Manufacture, Nanjing 210023, China.

[3]State Key Laboratory of Trauma, Burns and Combined Injury, Shock and Transfusion of Research Institute of Surgery, Daping Hospital, Army Medical University, Chongqing, China.

[≠]X. Ouyang and D. Zhu contributed equally to this work.

[*]To whom correspondence may be addressed. Email: xshen@njucm.edu.cn (Dr. X. Shen); liwenjun@njucm.edu.cn (Dr. W. Li); wangjy@njucm.edu.cn (Dr. J. Wang)

Highlights

- Selective inhibition of MAOB shows promise as a therapeutic strategy for PIPN.
- Khellin as a selective MAOB inhibitor ameliorated PIPN-like pathology in mice.
- Khellin alleviated apoptosis and improved mitochondrial dysfunction of DRG

neurons.

- Khellin inhibited astrocytes activation in spinal cord of PIPN mice.
- Khellin suppressed neuroinflammation through MAOB/NF-κB/NLRP3/ASC/Caspase1 pathway.

Graphical abstract

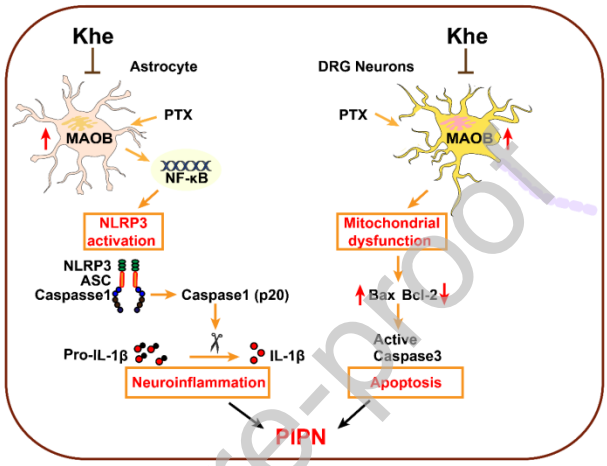

Abstract

Background: Treatment of paclitaxel (PTX)-induced peripheral neuropathy (PIPN) is full of challenges because of the unclear pathogenesis of PIPN. Herbal folk medicine Khellin (Khe) is a natural compound extracted from *Ammi visnaga* for treatment of renal colics and muscle spasms.

Purpose: Here, we aimed to assess the potential of Khe in ameliorating PIPN-like pathology in mice and investigate the underlying mechanisms.

Methods: PIPN model mice were conducted by injection of PTX based on the published approach. The capability of Khe in ameliorating the PTX-induced neurological dysfunctions was assayed by detection of nociceptive hypersensitivities including mechanical hyperalgesia, thermal hypersensitivity, and cold allodynia in

mice. The underlying mechanisms were investigated by assays against the PIPN mice with *MAOB*-specific knockdown in spinal cord and dorsal root ganglion (DRG) tissues by injection of adeno-associated virus (AAV)-*MAOB-shRNA*.

Results: We determined that MAOB not MAOA is highly overexpressed in the spinal cord and DRG tissues of PIPN mice and Khe as a selective MAOB inhibitor improved PIPN-like pathology in mice. Khe promoted neurite outgrowth, alleviated apoptosis, and improved mitochondrial dysfunction of DRG neurons by targeting MAOB. Moreover, Khe inhibited spinal astrocytes activation and suppressed neuroinflammation of spinal astrocytes via MAOB/NF-κB/NLRP3/ASC/Caspase1/IL-1β pathway.

Conclusion: Our work might be the first to report that MAOB not MAOA is selectively overexpressed in the spinal cord and DRG tissues of PIPN mice, and all findings have highly addressed the potency of selective MAOB inhibitor in the amelioration of PIPN-like pathology and highlighted the potential of Khe in treating PTX-induced side effects.

Keywords: PIPN, Khellin, MAOB, Apoptosis, Inflammation

Abbreviations: **AAV:** Adeno-associated virus; **BSA**: Bovine serum albumin; **DRG:** Dorsal root ganglion; **IENF**: Intraepidermal nerve fiber; **MAOs**: Monoamine oxidases; **MAOA**: Monoamine oxidase A; **MAOB**: Monoamine oxidase B; **ALS:** Amyotrophic lateral sclerosis; **MBP**: Myelin basic protein; **MMP**: Mitochondrial membrane potential; **mPTP**: Mitochondrial permeability transition pore; **NLRP3**: the Nod-like receptor protein 3; **OCR**: Oxygen consumption rate; **PDL**:

Poly-d-L-ornithine hydrobromide; **PIPN**: Paclitaxel-induced peripheral neuropathy; **PS**: Penicillin-streptomycin; **PTX:** Paclitaxel; **SCDH:** Spinal cord dorsal horn; **TMRM**: Tetramethyl rhodamine methyl ester; **TV**: Tumor volume; **GFAP**: Glial fibrillary acidic protein; **Iba1**: Ionized calcium binding adapter molecule 1

Introduction

Paclitaxel (PTX) as a first-line chemotherapeutic agent is widely used to treat solid neoplasms including ovarian, breast, and lung cancers. PTX-induced peripheral neuropathy (PIPN) is a common serious side effect with clinical hallmarks of tingling, burning pain, and numbness in feet and hands of the patients (Li et al., 2021). Such sensory abnormalities and pain symptoms of PIPN occur among 40 to 60% of patients with PTX treatment (Yang et al., 2021), seriously affecting the life quality of the patients. However, the pathogenesis of PIPN is complicated and unclear, and there is yet no optimal treatment against PIPN although conventional treatments such as nonsteroidal anti-inflammatory drugs, opioids, corticosteroids, and antidepressants are marginally effective in PIPN treatment (Li et al., 2021). It is thus valuable to develop new therapeutical strategies for PIPN.

Currently, emerging evidence has indicated that spinal astrocytes and microglia play a potent role in mediating nerve injury and inflammation (Liu et al., 2020; Milligan and Watkins, 2009), and astrocytes activation in spinal cord dorsal horn (SCDH) is tightly implicated in the pathogenesis of PIPN (Zhang et al., 2012). It was reported that activation of astrocytes results in the production of pro-inflammatory cytokines and chemokines (*e.g.*, IL-1β, TNF-α, IL-17 and CXCL-12) that are potent

neuromodulators in neuroinflammation and neuronal excitability (Li et al., 2021). Notably, the Nod-like receptor protein 3 (NLRP3) inflammasome as a pivotal sensor of these cytokines is a complex composed of NLRP3, ASC and cysteine protease caspase-1, and its activation promotes IL-1β and IL-18 precursors into their mature active forms (Sanchez-Rodriguez et al., 2021). Moreover, studies have demonstrated that PTX promotes the processing and releasing of IL-1β that is resulted from the ROS-induced activation of NLRP3 inflammasome (Jia et al., 2017).

Monoamine oxidases (MAOs) are flavin adenine dinucleotide-dependent mitochondrial enzymes responsible for catalyzing the oxidative deamination of structurally diverse amines in neurons and glial cells with production of aldehydes, ammonia and H_2O_2. MAOs have two isoforms, monoamine oxidase A and B (MAOA and MAOB) with different substrate specificity to each other (Sanchez-Rodriguez et al., 2021). MAOA preferentially deaminates serotonin and MAOB oxidizes β-phenylethylamine and benzylamine, although they commonly show similar affinities to dopamine, norepinephrine, epinephrine, tryptamine, and tyramine in most species (Hussain et al., 2018). MAO inhibitors have been determined to exhibit potentially beneficial effects on a series of neurological diseases including depression (Shulman et al., 2013), Parkinson's disease (Bar-Am et al., 2015), Alzheimer's disease (Chun et al., 2020), amyotrophic lateral sclerosis (ALS) (Sanchez-Rodriguez et al., 2021) and stroke (Sivenius et al., 2001). MAO activation increases H_2O_2 production that is a major source of oxidative stress, which is a main mechanism underlying cell apoptosis (Hussain et al., 2018). It was reported that in LPS/ATP-stimulated murine

bone marrow-derived macrophages, MAOB-derived ROS is indispensable for sustaining IL-1β secretion through NF-κB signaling that is involved in the priming step of NLRP3 inflammasome activation (Sanchez-Rodriguez et al., 2021). In addition, MAOB is also implicated in astrocytes activation in Alzheimer's disease (Chun et al., 2020). However, no report has yet been published on whether MAOs are linked to astrocytes-associated neuroinflammation induced by PTX in the spinal cord.

In the current work, we determined that MAOB not MAOA is selectively overexpressed in the spinal cord and dorsal root ganglion (DRG) tissues of PIPN mice and the herbal folk medicine Khellin (Khe, Fig. 2A) as a selective MAOB inhibitor effectively improved the PIPN-like pathology, and the underlying mechanisms have been intensively investigated. Our findings have highly addressed that selective inhibition of MAOB shows promise as a therapeutical strategy for PIPN and highlighted the potential of Khe in the treatment of such a clinical PTX-induced adverse reaction.

Materials and Methods

Cell culture

Primary DRG neurons dissected from normal or PIPN mice (Zhu et al., 2020) and primary astrocytes dissected from the spinal cord of newborn mice (postnatal days within 24 h) (Morioka et al., 2019) were prepared by published approaches.

Human breast cancer cell MCF7 was cultured in high-glucose DMEM medium (Corning, New York, USA) supplemented with 10% FBS and 100 U/mL PS.

All cells were maintained in a humidified incubator with 5% CO_2 at 37℃.

MTT assay

DRG neurons or MCF7 cells were seeded in 96-well plates and cultured overnight, followed by incubation with 300 nM PTX (MCE, Shanghai, China) or/and 10 μM Khe (purity > 99.92%, Target Mol, Washington, USA) for 24 h. Then, 0.5 mg/mL MTT was added into the plates and incubated with the cells for 4 h. Finally, the formazan crystals were dissolved in 150 μL DMSO and shook 15 min at room temperature. The absorbance was measured at 490 nm.

Neurite outgrowth measurement

The DRG neurons from normal mice were seeded in 12-well plates and treated with 300 nM PTX or/and 10 μM Khe for 24 h, while the DRG neurons isolated from PIPN mice were seeded in 12-well plates overnight. Subsequently, total neurite outgrowth was detected by the published approach (Zhu et al., 2020). DRG neurons were visualized using a fluorescence microscope (Lecia, Germany), and the neurite outgrowth measurement was performed by Image J.

Mitochondrial function assessment

Mitochondrial respiration was evaluated by XF24 Analyzer (Seahorse Biosciences, USA) according to the published approach (Zhu et al., 2020). Briefly, DRG neurons from PIPN mice were incubated in specialized 24-well plates. One hour before the detection, the medium was replaced with XF medium supplemented with 1 mM pyruvate (Gibco, Grand Island, New York, USA), 2 mM L-glutamine and 10 mM D-glucose. Then, 1 μM oligomycin, 1 μM carbonyl cyanide 4-(trifluoromethoxy) phenylhydrazone (FCCP) and a mixture of 1 μM rotenone and 1 μM antimycin A

were added sequentially into the Seahorse Flux Pak cartridges to measure oxygen consumption rate (OCR), basal respiration, maximal respiration, ATP production and spare respiratory capacity of DRG neurons.

Mitochondrial membrane potential (MMP) assay

DRG neurons from normal mice were seeded in 96-well plates and treated with 300 nM PTX or/and 10 μM Khe for 24 h. DRG neurons isolated from PIPN mice were seeded in 96-well plates overnight. Then, cells were incubated with 50 nM tetramethyl rhodamine methyl ester (TMRM, Invitrogen, California, USA) at 37℃ for 30 min. TMRM fluorescence was determined using fluorescent microscope reader (excitation wavelength at 548 nm, emission wavelength at 574 nm).

ROS determination in DRG neurons

DRG neurons from normal mice were seeded in 96-well plates and treated with 300 nM PTX or/and 10 μM Khe for 24 h. After refreshing the medium, 10 μM ROS fluorescent probe solution DCFH-DA were added into the plates and incubated at 37℃ for 20 min. Then the level of fluorescence (excitation wavelength at 488 nm, emission wavelength at 525 nm) was detected by a fluorescence microscope reader (Sekiguchi et al., 2018).

TUNEL assay

DRG neurons from normal mice were seeded in 24-well glass slides and treated with 300 nM PTX or/and 10 μM Khe for 24 h. DRG neurons isolated from PIPN mice were seeded in 24-well glass slides overnight. Subsequently, neuronal apoptosis was detected with TUNEL Apoptosis Assay Kit (Beyotime, Shanghai, China) according to

the manufacturer's instructions. DRG neurons were visualized by fluorescence microscopy and quantified by Image J.

Monoamine oxidase activity assay *in vivo*

The spinal cord tissues were homogenized with PBS on ice, and concentration of spinal cord homogenates was measured by BCA and adjusted to 2 mg/mL. Enzymatic activity assays were performed with the Amplex Red Monoamine Oxidase Assay Kit (Invitrogen, California, USA) according to the manufacturer's instructions. The fluorescence (excitation wavelength at 530 nm, emission wavelength at 590 nm) was measured with the fluorescence microplate reader (Umbarkar et al., 2015).

MAOB enzymatic activity assay *in vitro*

MAOB inhibition assay was performed using Monoamine Oxidase B Inhibition Screening Kit (Sigma-Aldrich, Missouri, USA) according to the manufacturer's instructions. MAOB enzyme solution (50 μL) was incubated with the test compounds (10 μL, S) for 10 min at 37℃ in a flat, black-bottomed 96-well plate in the dark. Then, 40 μL MAOB substrate solution was added into each well. MAOB assay buffer (10 μL) was used as Enzyme Control (EC). The fluorescence was measured by a fluorescence microplate reader (excitation wavelength at 535 nm, emission wavelength at 587 nm) at 37℃ for 10-40 min. Two time points (T1 and T2) were chosen in the linear range of the plot and the corresponding fluorescence values (RFU1 and RFU2) were obtained. The slope of S and EC were calculated by dividing the net ΔRFU (RFU2 - RFU1) values by the time ΔT (T2 - T1). The known MAOB

inhibitor selegiline (Ng et al., 2017) was used as a positive control. Relative inhibition (%) was calculated as follows:

$$Relative\ inhibition\ (\%) = \frac{(slope\ of\ EC - Slope\ of\ S)}{Slope\ of\ EC} \times 100$$

siRNA plasmid transfection

Primary DRG neurons or astrocytes were transfected using Lipofectamine 2000 (Invitrogen, Carlsbad, California, USA) by manufacturer's protocols, and *si*-negative control (*si-NC*) was used as a negative control. Briefly, *si-NC* or *si-MAOB* was dissolved in 25 μL Opti-MEM medium (Gibco, Grand Island, New York, USA) and mixed with Lipofectamine 2,000. The mixture was then added into cells. After 6 h, culture media were refreshed with DMEM/F-12 medium supplemented with 10% FBS and 100 U/mL PS. The knockdown efficiency of *si-MAOB* was detected by western blot assay 48 h after *si-MAOB* treatment and the second sequence was chosen for the following MAOB *siRNA* related experiments based on its highest efficiency in knocking down MAOB (Fig. S1A-B).

RNA oligonucleotides used for siRNA are listed in Table S1.

Animals

Male C57BL/6N mice (7-8 weeks) and female NU/NU Nude mice (4-5 weeks) were purchased from Vital River Laboratory Animal Technology Co (Beijing, China) and maintained under standard conditions at room temperature (22℃) by a 12 h light/dark cycle. According to National Institutes of Health guidelines, all animal experiments were approved by the Animal Ethics Committee of Nanjing University of Chinese Medicine.

PIPN mice- PIPN model mice were conducted as described previously (Yang et al., 2021). Briefly, PTX (6 mg/mL in 50% cremophor EL and 50% ethanol) was diluted in sterile saline to a final concentration of 0.4 mg/mL and *i.p.* injected to male C57BL/6N mice at a dose of 4 mg/kg on day 0, 2, 4, and 6 with a final cumulative dose of 16 mg/kg. The PIPN mice were eligible with symptoms of reductions of 50% mechanical threshold, paw thermal response latency and paw cold response latency compared with normal male C57BL/6N mice (ethical approval number: No. 202001A025, approved on Apr 16th, 2020).

AAV-induced MAOB knockdown mice- AAV-induced MAOB knockdown mice were obtained via intrathecally injection of adeno-associated virus (AAV)-*MAOB-shRNA* (AAV-*MAOB-shRNA*, WZ Biosciences Inc, Shandong, China) (The titer of AAV-*MAOB-shRNA* was 6.92×10^{13} vg/mL) into the L4-L6 subarachnoid space of the spinal cord before the first PTX *i.p.* injection according to the published approach (Nie et al., 2018) (ethical approval number: No. 202008A025, approved on Sep 2nd, 2020). shRNA oligonucleotides used for AAV-*shRNA* are listed in Table S2. 21 days after AAV injection, expressions of MAOB in the spinal cord and DRG tissues from mice were detected by western blot assay. The results showed that the expressions of MAOB were decreased by 48% in spinal cord and 38% in DRG tissues with AAV-*MAOB-shRNA* treatment (Fig. S1C-D).

Tumor xenograft model mice- MCF7 cells (3.5×10^7 cells) were subcutaneously implanted in the armpits of female NU/NU Nude mice. The mice with tumor size of 80-100 mm^3 were classified as tumor xenograft model mice. Tumor volume (TV) was

measured by a vernier caliper and calculated using the following formula: TV (mm^3) = $D/2 \times d^2$ (D: longest diameter; d: shortest diameters) (ethical approval number: No. 202007A012, approved on July 14th, 2020).

Drugs and experimental groups

Khe was dissolved in sterile saline with 4% DMSO and 2% tween-80 (Sigma-Aldrich, Missouri, USA). Experimental mice were *i.p.* treated with vehicle (sterile saline contained 4% DMSO and 2% tween-80) or Khe.

PIPN model mice were randomized into PTX group (PIPN model mice treated with vehicle), PTX + Khe-7 group (PIPN model mice treated with Khe-7 mg/kg/day) and PTX + Khe-15 group (PIPN model mice treated with Khe-15 mg/kg/day) (n = 10/group). Normal male C57BL/6N mice treated with the same amount of vehicle were set as Control group in the assay. Mice administrations were performed for 4 weeks, once a day.

AAV-injected mice were randomized into AAV-*NC*+Veh group (AAV-*NC*-injected mice treated with vehicle), AAV-*NC*+PTX group (AAV-*NC*-injected mice treated with PTX), AAV-*MAOB*+Veh group (AAV-*MAOB*-injected mice treated with vehicle), AAV-*MAOB*+PTX group (AAV-*MAOB*-injected mice treated with PTX) and AAV-*MAOB*+PTX+Khe group (AAV-*MAOB*-injected mice treated with PTX and Khe-15 mg/kg/day) (n = 12/group). 3 weeks after AAV injection, 4 mg/kg PTX was *i.p.* injected every other day for 4 times to establish the PIPN mice model. Then Khe or vehicle was administrated for 4 weeks, once a day.

Tumor xenograft model mice were randomized into Control group (tumor xenograft model mice treated with vehicle), PTX group (tumor xenograft model mice treated with PTX), PTX+Khe-15 group (tumor xenograft model mice treated with PTX and Khe-15 mg/kg/day) and Khe-15 group (tumor xenograft model mice treated with Khe-15 mg/kg/day) (n = 7/group). When tumor size reached approximately 80-100 mm^3, 4 mg/kg PTX was *i.p.* injected every other day for 4 times, then Khe (15 mg/kg/day) or vehicle was administrated for 4 weeks, once a day.

At the end of the animal experiments, the mice were anesthetized with 5% isoflurane and then sacrificed.

Behavioral experiments

Mechanical hyperalgesia measurement- Von Frey filaments (Ugo Basile, Comerio VA, Italy) was used to detect mechanical sensitivity of mice (Zhu et al., 2020). Briefly, mice were allowed to stand on a metal mesh grid for 15 min. The right hind paw plantar surface of each mouse was stimulated by Von Frey filaments with forces ranging from 0.4 to 2.0 g. A paw withdrawal response including scratching, licking, and raising the foot pad were considered the positive responses. The 50% pain threshold of PIPN mice was calculated using the following formula: 50% threshold = 10^ $[X_f + k\delta]/10000$, where X_f is the corresponding force coefficient measured by Von Frey wire, k represents the reference of the positive/negative reaction parameter table in the Up and Down method, $\delta = 0.224$.

Thermal hypersensitivity measurement- A thermal stimulation meter was employed to evaluate the sensitivity of mice against heat according to the published

method (Nie et al., 2018). Briefly, mice were placed on the platform of thermal apparatus (Ugo Basile, Comerio VA, Italy) and stayed for 15 min before the test. The paw withdrawal latency was then assessed and the continuous time of the heat radiation at 50℃ was recorded. If the mice appeared the response of withdrawal, the record was stopped.

Cold allodynia measurement- Cold allodynia was employed to evaluate the sensitivity of mice against cold according to the published method (Li et al., 2017). Each mouse was placed in a cold aluminum plate (Ugo Basile, Comerio VA, Italy) and stayed for 15 min before the experiment. The paw withdrawal latency was then assessed by the cold testing apparatus and the continuous time of the cold radiation at 4℃ was recorded. If the mice appeared the response of withdrawal, the instrument record was stopped.

The paw withdrawal latency of each mouse was calculated 3 times and the interval between each was 10 minutes, while the average value was calculated for statistical analysis (Chen et al., 2013). All responses were scored by an experimenter blinded to injection condition and experimental cohort.

Western blot assay

Cell-based assay- Primary DRG neurons were incubated with PTX (300 nM) and different concentrations of Khe (0, 5 and 10 μM) for 24 h. Primary astrocytes from spinal cord were incubated with PTX (5 μM) and different concentrations of Khe (0, 5 and 10 μM) for 3.5 h, ATP (3 mM) was then added and incubated for another 0.5 h. Primary DRG neurons and astrocytes were lysed with RIPA buffer

containing protease inhibitor cocktail and phosphatase inhibitor cocktail on ice for 20 min, followed by centrifugation at 12,000 rpm for 30 min at 4℃.

Spinal cord and DRG tissues-based assay- Spinal cord and DRG tissues from mice were lysed with RIPA buffer containing protease inhibitor cocktail and phosphatase inhibitor cocktail. After the tissues were lysed completely, the homogenates were centrifuged at 12,000 rpm for 30 min at 4℃.

Western blot assay was performed as previously described (Zhu et al., 2020). The blots were developed and visualized using a ChemiDoc MP (Bio-Rad, Hercules, California, USA).

The antibodies used in this study were listed in Table S3.

RNA isolation and quantitative real-time PCR (qRT-PCR) assay

Total RNA was extracted using RNAiso plus regent (TaKaRa, Otsu City, Japan) by manufacturer's protocol. 1 μg RNA was then used to synthesize cDNA by the High-Capacity cDNA reverse transcription kit (Takara Biomedical Technology Co, Beijing, China). Finally, mRNA levels of different genes were quantified by qRT-PCR assay using SYBR Green Master Mix (Vazyme, Nanjing, China). β-actin was used as the endogenous reference gene.

The primers used in qRT-PCR were listed in Table S4.

Immunofluorescence assay

Primary astrocytes- Primary astrocytes grown on slides were washed three times and fixed in 4% paraformaldehyde for 5 min at room temperature. The cells were incubated with 0.3% Triton X-100 for 10 min and blocked with 4% BSA for 30 min at

room temperature, followed by incubating with anti-GFAP antibody (1:1,000) and anti-NF-κB antibody (1:500) overnight at 4℃. The slides were washed three times and incubated with fluorescent secondary detection antibodies (dilution 1:250) goat anti-rabbit and goat anti-mouse for 2 h and the nuclear was stained with Hoechst 33342.

Tissues- The spinal cord tissues and foot pad of hind limb were dissected and fixed in 4% paraformaldehyde for 24 h, whereas sciatic nerve was fixed in 2.5% glutaraldehyde (EM Grade), and then cryoprotected in 30 % sucrose solution for 48 h at 4℃. All tissues were sectioned (10 μm) using a cryostat (Leica, Germany) and mounted on glass slides. The slides were incubated in 5% Triton X-100 for 10 min and blocked in 5% BSA for 30 min at room temperature, followed by incubating overnight at 4℃ with appropriate primary antibody. The slides were then washed three times and incubated with fluorescent secondary detection antibodies (dilution 1:250) for 2 h and the nuclear was stained with Hoechst 33342.

Images were acquired using a Leica fluorescence microscope and analyzed by Image J. The antibodies used for immunostaining were listed in Table S5.

Determination of PTX level

PTX was quantified using LC/MS/MS (Leblanc et al., 2018). Spine cord was extracted at 0, 2, 4, 6, 12, 24 h after the fourth injection of PTX. Spine cord tissues for the quantification of PTX were prepared by extraction of 1 mL methyl alcohol. After vigorous mixing and centrifugation for 10 minutes at 12,000 g, the supernatant was evaporated by a centrifugal freeze concentrator (Labconco, USA). The residue was

dissolved in 100 μL water, from which aliquots of 30 μL were injected into the LC/MS/MS system. Sample extracts were injected into an Alltima HP C18 HL 3-μm column (50 × 2.1 mm internal diameter, Alltech Applied Science) by a Waters 2795 Separation Module. The mobile phase for determination of PTX was composed of acetonitrile and water containing formic acid (0.1% v/v), and was delivered using linear gradient settings at a flow rate of 0.2 mL/min. Detection was performed with a triple quadrupole liquid-mass spectrometry (Sciex, USA) in the positive ion mode. The electrospray ionization was set at 3.8 kV and the cone voltage at 18 V. The dwell times were set at 150 ms and the interchannel delay at 50 ms. A multiple-reaction monitoring (MRM) mode was applied for the quantification with the following parameters: m/z 854→286, collision energy at 20 eV for paclitaxel. The collision cell pressure was set at approximately 4×10^{-3} mbar (argon). The within-run and between-run precisions were within 7.14%, while the accuracy ranged from 88.5% to 94.1%.

Statistical analysis

All data were expressed as mean ± SEM and analyzed by GraphPad Prism version 7.0. The sample size for each experiment was indicated in the figure legends. Unpaired 2-tailed Student's t-test was used for two-group comparison. One-way ANOVA with Dunnett's post-hoc test and two-way ANOVA with Bonferroni post hoc test were used for at least three group's comparisons. In cases when the data appeared to be non-normally distributed, a normality test was performed

(Kolmogorov-Smirnov), followed by a non-parametric Mann-Whitney test. $p < 0.05$ was considered statistically significant.

Results

MAOB was selectively overexpressed in the astrocytes of spinal cord and neurons of DRG tissues of PIPN mice

MAOB was selectively overexpressed in the spinal cord and DRG tissues of PIPN mice- qRT-PCR and western blot results indicated that the mRNA and protein levels were unchanged for MAOA but upregulated for MAOB in the spinal cord and DRG tissues of PIPN mice compared with those of control mice (C57BL/6N mice) (Fig. 1A-F).

Additionally, the assay results by commercial MAO enzymatic activity assay kit also demonstrated that the enzymatic activity was upregulated for MAOB but unchanged for MAOA in the spinal cord and DRG tissues of PIPN mice compared with those of control mice (Fig. 1G-H).

MAOB was selectively overexpressed in the astrocytes of spinal cord and neurons of DRG tissues- Immunofluorescence results indicated that MAOB was colocalized primarily with astrocytes (glial fibrillary acidic protein (GFAP) as an astrocytic marker (Liu et al., 2020), Fig. 1I-J) and rarely with neurons (NeuN as a neuronal marker (Liu et al., 2020), Fig. S2A-B) or microglia (ionized calcium binding adapter molecule 1 (Iba1) as a microglial marker (Liu et al., 2020), Fig. S2C-D) in SCDH, while mainly colocalized with neurons (β-tubulin as a neuronal marker (Jhaveri et al., 2018), Fig. 1K-L) and rarely with macrophage (CD68 as a macrophage

marker (Chistiakov et al., 2017), Fig. S2E-F) in DRG tissues of PIPN mice. Obviously, MAOB was selectively overexpressed in the astrocytes of spinal cord and neurons of DRG tissues in PIPN mice (Fig. 1I-L).

Accordingly, further experiments in primary neurons of DRG tissues and astrocytes of the spinal cord were performed to explore the potential of MAOB in mediating PIPN *in vitro*.

Khe was determined to be a selective MAOB inhibitor

Since we have determined the selective overexpression of MAOB in PIPN mice, we next identify whether selective MAOB inhibition may improve PIPN-like pathology in mice. In the assay, we at first screened the lab in-house approved drug library for selective MAOB inhibitors (over MAOA) and Khe was finally obtained (Fig. 2A). As indicated in Fig. 2B, Khe inhibited MAOB activity by IC_{50} at 9.162 μM.

Next, to verify the selectivity of Khe against MAOB, we detected the inhibition of Khe against MAOA and MAOB enzymatic activities in the spinal cord and DRG tissues of PIPN mice by commercial MAO enzymatic activity assay kit. The results indicated that the enzymatic activity of MAOB not MAOA was inhibited in the spinal cord or DRG tissues of Khe-treated PIPN mice compared with that of PIPN mice (Fig. 2C-D). In addition, qRT-PCR and western blot assay results also indicated that Khe selectively inhibited the mRNA and protein levels of MAOB not MAOA in the spinal cord or DRG tissues of PIPN mice (Fig. 2E-J).

Thus, all results revealed that Khe was a selective inhibitor of MAOB.

Khe protected DRG neurons from PTX-induced damage by targeting MAOB

Given that DRG neuronal damage is highly related to PIPN pathology, we detected the effects of Khe on mitochondrial dysfunction, neurite outgrowth and apoptosis in PTX-induced DRG neurons with anti-PIPN clinic drug duloxetine (Dul) (Lu et al., 2020; Meng et al., 2019) as a positive control.

We at first detected the effect of Dul on cell vitality of DRG neurons, and MTT assay result demonstrated that Dul rendered no influences on DRG neuronal vitality at 100, 150 and 300 nM (Fig. S3A), which was consistent with the previous reports (Lu et al., 2020; Meng et al., 2019). Therefore, 300 nM Dul was set as a positive control in the following experiments.

Khe protected DRG neurons from PTX-induced mitochondrial dysfunction by targeting MAOB- MTT assay results indicated that Khe protected DRG neurons from PTX-induced neurotoxicity (Fig. 3A). In addition, Khe antagonized the PTX-induced ROS upregulation (Fig. 3B) and MMP downregulation (Fig. 3C) in DRG neurons, whereas Dul was less effective compared with Khe. Notably, *si-MAOB* deprived Khe of its above-mentioned neuroprotective capabilities (Fig. 3D-F).

Khe protected DRG neurons from PTX-induced axonal damage by targeting MAOB- Next, by considering that axonal damage and degeneration are tightly associated with PIPN pathology (Pease-Raissi et al., 2017), we detected the effect of Khe on the neurite outgrowth of DRG neurons. Immunofluorescence results indicated that PTX inhibited the neurite outgrowth of DRG neurons, and Khe was more effective than Dul in antagonizing the PTX-induced inhibition against the neurite

outgrowth (Fig. 3G-H). Notably, *si-MAOB* deprived Khe of its above-mentioned antagonistic capability (Fig.3I-J).

Khe protected DRG neurons from PTX-induced apoptosis by targeting MAOB- It was reported that increased expression or activity of MAOB might cause ROS accumulation inducing the opening of mitochondrial permeability transition pore (mPTP) and release of apoptogenic factors ultimately leading to apoptosis (Sorato et al., 2014). TUNEL assay result demonstrated that Khe and Dul both antagonized PTX-induced apoptosis in primary DRG neurons, whereas Dul was less effective compared with Khe (Fig. 3K-L), and western blot results indicated that Khe antagonized the PTX-induced downregulation of anti-apoptotic protein Bcl-2 and upregulation of pro-apoptotic proteins Bax and C-caspase3 in PTX-treated DRG neurons (Fig. 3O-P). Notably, *si-MAOB* deprived Khe of its above-mentioned anti-apoptotic effects (Fig. 3M-N and Q-R).

Together, all results implied that Khe protected DRG neurons from PTX-induced damage by targeting MAOB.

Khe suppressed neuroinflammation in PTX/ATP-treated primary astrocytes via MAOB/NF-κB/NLRP3/ASC/Caspase1/IL-1β pathway

Neuroinflammation is highly implicated in the pathology of PIPN and PTX induces the production of pro-inflammatory cytokines (*e.g.*, TNF-α, IL-1β) in spinal cord (Liu et al., 2019). Additionally, PTX also induces activation of caspase-1 *in vivo* in the presence of NLRP3 inflammasome-activating signal such as ATP (Son et al., 2019). Thus, we inspected the anti-inflammatory potential of Khe in PTX/ATP-treated

primary astrocytes.

Khe repressed neuroinflammation in PTX/ATP-treated primary astrocytes by targeting MAOB- qRT-PCR results indicated that Khe was more effective than Dul in antagonizing the PTX/ATP-induced increases in mRNA levels of IL-1β and TNF-α (Fig. 4A) and *si-MAOB* deprived Khe of such antagonistic capabilities in primary astrocytes (Fig. 4B). All results demonstrated that Khe repressed neuroinflammation in PTX/ATP-treated primary astrocytes by targeting MAOB.

Khe inhibited NLRP3 inflammasome activation in PTX/ATP-treated primary astrocytes by targeting MAOB- NLRP3 inflammasome becomes activated when exposed to stimuli, in that NLRP3 undergoes a conformational change and assembles with adaptor protein ASC and pro-Caspase 1 resulting in activation of caspase 1 and further formation of mature IL-1β (Sanchez-Rodriguez et al., 2021). Here, we examined the potential of Khe in inhibiting NLRP3 inflammasome activation in primary astrocytes. Both western blot (Fig. 4C-D) and qRT-PCR (Fig. 4E) results demonstrated that Khe antagonized the PTX/ATP-induced increases in protein levels of NLRP3 and cleaved caspase-1 (p20) (Cas1 (p20)) as well as mRNA level of NLRP3 in primary astrocytes. Notably, *si-MAOB* deprived Khe of its above-mentioned antagonistic capabilities (Fig. 4F-H). Thus, all results demonstrated that Khe inhibited NLRP3 inflammasome activation in PTX/ATP-treated primary astrocytes by targeting MAOB.

Khe suppressed NF-κB activation in PTX/ATP-treated primary astrocytes by targeting MAOB- By considering that NF-κB as a vital nuclear transcription factor

functions potently in mediating NLRP3 transcription (Sanchez-Rodriguez et al., 2021), regulation of Khe against NF-κB activation was inspected in PTX/ATP-treated primary astrocytes.

Western blot (Fig. 4I-J) and immunofluorescence (Fig. 4K-L) results indicated that Khe antagonized the PTX/ATP-induced increases in protein levels of NF-κB/p-NF-κB and NF-κB nuclear translocation in primary astrocytes. Moreover, *si-MAOB* deprived Khe of its antagonistic capability against NF-κB (Fig. 4M-N). These results demonstrated that Khe suppressed NF-κB activation in PTX/ATP-treated primary astrocytes by targeting MAOB.

NF-κB signaling was required for Khe inhibition against NLRP3 inflammasome activation in PTX/ATP-treated primary astrocytes- Next, NF-κB inhibitor pyrrolidyl dithiocarbamate (PDTC, Sigma-Aldrich, Missouri, USA) (Ambrosini et al., 2019) related assay was performed. As shown in Fig. 4O-R, PDTC deprived Khe of its capability in antagonizing the PTX/ATP-induced upregulation of mRNA levels of IL-1β, TNF-α and NLRP3, and protein levels of NLRP3 and Cas1 (p20) in primary astrocytes.

Together, all results indicated that Khe suppressed neuroinflammation in PTX/ATP-treated primary astrocytes via MAOB/NF-κB/NLRP3/ASC/Caspase1/IL-1β pathway.

Khe treatment ameliorated neurological dysfunctions in PIPN mice by targeting MAOB

To investigate the capability of Khe in ameliorating neurological dysfunctions in

PIPN mice, behavior tests (mechanical hyperalgesia, thermal hypersensitivity, and cold allodynia) were performed against PIPN mice by treatment of Khe (7, 15 mg/kg/day). Moreover, to verify the above-mentioned ameliorative effects of Khe through targeting MAOB, the related assays were also performed in PIPN mice with *MAOB*-specific knockdown in the spinal cord and DRG tissues by injection of AAV-*MAOB-shRNA* (Fig. 5A-B).

As indicated in Fig. 5C-E, PIPN mice exhibited repression of mechanical hyperalgesia (Fig. 5C), thermal hypersensitivity (Fig. 5D) and cold allodynia (Fig. 5E) compared with control mice, and Khe treatment ameliorated all neurological dysfunctions in PIPN mice (Fig. 5C-E). It was noted that AAV-*MAOB-shRNA* injection improved mechanical hyperalgesia, thermal hypersensitivity, and cold allodynia in PIPN mice and Khe treatment had no impacts on neurological dysfunctions in AAV-*MAOB-shRNA* injected PIPN mice (Fig. 5F-H).

Collectively, all results suggested that Khe treatment ameliorated neurological dysfunctions in PIPN mice by targeting MAOB, while rendering no influences on body weight and food intake in mice (Fig. S3B-E).

Khe treatment enhanced the neurite outgrowth of DRG neurons from PIPN mice by targeting MAOB

Immunostaining results demonstrated that the neurite outgrowth of DRG neurons was repressed from PIPN mice compared with that from control mice, while enhanced from Khe-treated PIPN mice compared with that from vehicle-treated PIPN mice (Fig. 5I-J).

Notably, the neurite outgrowth of DRG neurons from AAV-*MAOB-shRNA* injected PIPN mice was obviously upregulated compared with that from AAV-*NC-shRNA* injected PIPN mice, and Khe treatment had no impacts on the neurite outgrowth of DRG neurons from AAV-*MAOB-shRNA* injected PIPN mice (Fig. 5K-L).

Thus, all results demonstrated that Khe treatment enhanced the neurite outgrowth of DRG neurons from PIPN mice by targeting MAOB.

Khe treatment improved the peripheral nerve structure and vascular function in PIPN mice by targeting MAOB

Khe treatment improved the peripheral nerve structure in PIPN mice by targeting MAOB- Considering that intraepidermal nerve fiber (IENF) loss is one of the pathologic events of PIPN (Singhmar et al., 2018), immunofluorescence assay was performed and the results indicated that the number of fibers in foot pads was downregulated in PIPN mice compared with that in control mice, while Khe treatment upregulated the IENF density in PIPN mice (Fig. 6A-B). AAV-*MAOB-shRNA* injection upregulated the IENF density of foot pads in PIPN mice, and Khe treatment had no impacts on the IENF density in AAV-*MAOB-shRNA* injected PIPN mice (Fig. 6C-D). Thus, all results demonstrated that Khe treatment improved the peripheral nerve structure in PIPN mice by targeting MAOB.

Khe treatment improved the peripheral vascular function in PIPN mice by targeting MAOB- Microvascular damage was tightly involved in PTX-induced neuropathy (Kirchmair et al., 2007), and we examined the vascular function in sciatic

nerve and foot pads of mice by detecting blood flow velocity and blood perfusion area through Laser Speckle Contrast Imaging. The results indicated that the blood flow velocities (Fig. 6E-F and H-I) and blood perfusion areas (Fig. 6E, G, H and J) in PIPN mice were both repressed compared with those in control mice, while ameliorated in Khe-treated PIPN mice compared with those in vehicle-treated PIPN mice (Fig. 6E-J). Notably, AAV-*MAOB-shRNA* injection also increased the blood flow velocities and blood perfusion areas of sciatic nerve and foot pads in PIPN mice, but Khe treatment had no impacts on the blood flow velocity and blood perfusion area in AAV-*MAOB-shRNA* injected PIPN mice (Fig. 6K-P). All results thus indicated that Khe treatment improved the peripheral vascular function in PIPN mice by targeting MAOB.

Taken together, all results implied that Khe treatment improved the peripheral nerve structure and vascular function in PIPN mice by targeting MAOB.

Khe treatment protected the myelin sheath structure in PIPN mice by targeting MAOB

Demyelination and myelin damage of sciatic nerve were clinic hallmarks of PIPN (Scripture et al., 2006), and immunofluorescence assay results against myelin basic protein (MBP) indicated that Khe treatment suppressed the demyelination and increased the myelin sheath thickness of sciatic nerve in PIPN mice (Fig. 7A).

Notably, AAV-*MAOB-shRNA* injection ameliorated the demyelination and myelin damage of sciatic nerve in PIPN mice, while Khe treatment had no impacts on the myelin sheath structure in AAV-*MAOB-shRNA* injected PIPN mice (Fig. 7B).

Thus, all results demonstrated that Khe treatment protected the myelin sheath structure in PIPN mice by targeting MAOB.

Khe treatment improved the mitochondrial dysfunction of DRG neurons in PIPN mice by targeting MAOB

Given that PTX may cause mitochondrial dysfunction of DRG neurons (Duggett et al., 2017), we evaluated the regulation of Khe treatment against mitochondrial functions in DRG neurons of PIPN mice via Seahorse Bioscience XF24 analyzer. The results indicated that the levels of OCR (Fig. 7C), basal respiration (Fig. 7D), ATP production (Fig. 7E), maximal respiration (Fig. 7F) and spare respiratory capacity (Fig. 7G) were all downregulated in DRG neurons of PIPN mice, while Khe treatment antagonized the downregulation of all those mitochondria-associated parameters (Fig. 7C-G). Additionally, we also inspected MMP level in DRG neurons of PIPN mice and the result indicated that Khe treatment upregulated MMP level (Fig. 7H).

Notably, AAV-*MAOB-shRNA* injection upregulated all above-mentioned mitochondria-related parameters of DRG neurons in PIPN mice, but Khe treatment had no impacts on any of them in AAV-*MAOB-shRNA* injected PIPN mice (Fig. 7I-N).

Together, all results demonstrated that Khe treatment improved the mitochondrial dysfunction of DRG neurons in PIPN mice by targeting MAOB.

Khe treatment suppressed neuroinflammation of the spinal cord in PIPN mice via MAOB/NF-κB/NLRP3/ASC/Caspase1/IL-1β pathway

Khe treatment suppressed astrocyte activation of SCDH in PIPN mice by targeting MAOB- Astrocytes and microglia in SCDH play important roles in mediating chronic pain (Liu et al., 2020), and we performed immunofluorescence assay using GFAP and Iba1 as markers for astrocyte and microglia, respectively. The results indicated that the expression of GFAP (Fig. 8A-B) not Iba1 (Fig. S4A-B) was increased in SCDH of PIPN mice and Khe treatment suppressed astrocyte activation. Notably, AAV-*MAOB-shRNA* injection inhibited astrocyte activation of SCDH in PIPN mice and Khe treatment had no effects on astrocyte activation of SCDH in AAV-*MAOB-shRNA* injected PIPN mice (Fig. 8C-D). Thus, all results demonstrated that Khe treatment suppressed astrocyte activation of SCDH in PIPN mice by targeting MAOB.

Khe treatment repressed neuroinflammation of the spinal cord in PIPN mice by targeting MAOB- Astrocyte activation functions by releasing pro-inflammatory cytokines including IL-1β and TNF-α in PIPN mice (Liu et al., 2019). Here, qRT-PCR and western blot results indicated that either Khe treatment or AAV-*MAOB-shRNA* injection repressed the levels of IL-1β and TNF-α in the spinal cord of PIPN mice (Fig. 8E-L), while Khe treatment had no impacts on either of these two pro-inflammatory cytokines in the spinal cord of AAV-*MAOB-shRNA* injected PIPN mice (Fig. 8G-H and K-L). Thus, all results demonstrated that Khe treatment repressed neuroinflammation of the spinal cord in PIPN mice by targeting MAOB.

Khe treatment inhibited NLRP3 inflammasome activation of the spinal cord in PIPN mice by targeting MAOB- Both western blot (Fig. 8I-J) and qRT-PCR (Fig. 8M)

results indicated that Khe treatment suppressed the protein levels of NLRP3, pro-Caspase1, ASC and Cas1 (p20) as well as mRNA level of NLRP3, indicative of the suppression of NLRP3 inflammasome activation of the spinal cord in PIPN mice. Notably, AAV-*MAOB-shRNA* injection repressed NLRP3 inflammasome activation of spinal cord in PIPN mice and Khe treatment had no impacts on NLRP3 inflammasome activation in AAV-*MAOB-shRNA* injected PIPN mice (Fig. 8K-L and N). Thus, all results demonstrated that Khe treatment inhibited NLRP3 inflammasome activation of the spinal cord in PIPN mice by targeting MAOB.

Khe treatment suppressed NF-κB activation of the spinal cord in PIPN mice by targeting MAOB- Western blot (Fig. 8I-J) results demonstrated that Khe treatment inhibited the protein levels of NF-κB and p-NF-κB, and immunofluorescence result (Fig. 8O-P) indicated that Khe treatment suppressed NF-κB nuclear translocation of SCDH astrocytes in PIPN mice. Moreover, AAV-*MAOB-shRNA* injection inhibited NF-κB activation of SCDH astrocytes in PIPN mice and Khe treatment had no impacts on NF-κB activation in AAV-*MAOB-shRNA* injected PIPN mice (Fig. 8K-L and Q-R). Thus, all results demonstrated that Khe treatment suppressed NF-κB activation of the spinal cord in PIPN mice by targeting MAOB.

Collectively, all results demonstrated that Khe treatment suppressed neuroinflammation of the spinal cord in PIPN mice via MAOB/NF-κB/NLRP3/ASC/Caspase1/IL-1β pathway.

Khe treatment protected against DRG neuronal damage and apoptosis in PIPN mice by targeting MAOB

Khe treatment protected against DRG neuronal damage in PIPN mice by targeting MAOB- We at first evaluated the potential of neuronal damage of SCDH in PIPN mice by ATF3 (a neuronal damage marker) staining. As shown in Fig. S4C-D, we did not observe any ATF3 positively stained cells of SCDH in PIPN mice. Given that neuronal damage occurred in peripheral sensory neurons after PTX treatment (Peters et al., 2007), we next performed immunofluorescence assay against ATF3 in DRG neurons of PIPN mice and found that the number of ATF3 positively stained neurons was markedly increased, indicative of DRG neuronal damage (Fig. 9A-B). Notably, Khe treatment or AAV-*MAOB-shRNA* injection repressed ATF3 number of DRG neurons in PIPN mice, while AAV-*MAOB-shRNA* deprived Khe of its above-mentioned repressive capability in AAV-*MAOB-shRNA* injected PIPN mice (Fig. 9A-D). All results demonstrated that Khe treatment protected against DRG neuronal damage in PIPN mice by targeting MAOB.

Khe treatment protected against DRG neuronal apoptosis in PIPN mice by targeting MAOB- PTX induces not only neuronal damage but also neuronal apoptosis (Chine et al., 2019), and western blot assay results indicated that Khe treatment or AAV-*MAOB-shRNA* injection upregulated the expression of anti-apoptotic protein Bcl-2 and downregulated the expressions of pro-apoptotic protein Bax and C-caspase3, while AAV-*MAOB-shRNA* deprived Khe of its above-mentioned anti-apoptotic effect in DRG tissues of AAV-*MAOB-shRNA* injected PIPN mice (Fig. 9E-H). Thus, all results demonstrated that Khe treatment protected against DRG neuronal apoptosis in PIPN mice by targeting MAOB.

Taken together, all results implied that Khe treatment protected against DRG neuronal damage and apoptosis in PIPN mice by targeting MAOB.

Khe had no effects on the antitumor activity of PTX

Next, we investigated whether Khe had impacts on the antitumor activity of PTX. In the assay, the effect of Khe on the viability of PTX-treated MCF7 cells was at first inspected. MTT assay result indicated that PTX (300 nM) treatment expectedly reduced MCF7 cell viability (Fig. 10A), and Khe also inhibited the proliferation of MCF7 cells as reported previously (Amira Mohammed Beltagy, 2015), while Khe had no effects on the antitumor activity of PTX (Fig. 10B).

Moreover, the effect of Khe on PTX-mediated antitumor activity was detected *in vivo*. In the assay, we subcutaneously inoculated human breast cancer MCF7 cells into the NU/NU Nude mice and the tumors were excised and weighed after a 4-week growth period (Fig. 10C). The results demonstrated that PTX treatment decreased tumor weight (Fig. 10D) and volume (Fig. 10E), whereas Khe could slightly suppress tumor growth without affecting PTX-mediated antitumor activity (Fig. 10F).

All results indicated that Khe treatment had no effects on the antitumor activity of PTX.

Discussion

PIPN is a common and serious side effect during PTX treatment, and it is full of challenges to develop effective treatment against this clinical side effect. Currently, Dul, a norepinephrine reuptake inhibitor, was recommended as the only clinical drug for the treatment of CIPN induced by oxaliplatin and PTX by the American Society of

Clinical Oncology (Meng et al., 2019), although it was less effective for patients administered with paclitaxel (Kanbayashi et al., 2017). Additionally, Dul is also known to cause severe side effects, such as increased heart rate, GI disturbance, constipation, anorexia and dizziness (Burch, 2019). Other drugs such as tricyclic antidepressants (*e.g.*, amitriptyline) (Kautio et al., 2008) and anticonvulsants (*e.g.*, gabapentin) (Hu et al., 2019) have been used for treatment of PIPN, while they often have no significant efficacy or have systemic side effects (Hu et al., 2019). Thus, finding new therapeutic strategies for PIPN and elucidating its mechanism have become hotspots in the field of contemporary PIPN drug development.

Herbal folk medicine Khe was mainly extracted from *Ammi visnaga* for treatment of coronary diseases, bronchial asthma, renal colics and muscle spasms (Vrzal et al., 2013). In addition, Khe has been also reported on its anti-inflammatory, analgesic, antibacterial, antiviral and many other activities (Usmani et al., 2021), although the underlying mechanism has not yet been clear. Here, we uncovered that Khe efficiently ameliorated PIPN-like pathology in PIPN mice and demonstrated its underlying mechanism, which has not been reported to date.

MAOs as flavoproteins of the outer mitochondrial membrane are responsible for the oxidative deamination of biogenic and xenobiotic amines. The two isoforms MAOA and MAOB of MAOs play different biological roles due to their different substrate specificities (Sanchez-Rodriguez et al., 2021). MAOB has been considered an important target in the treatment of Parkinson's disease, while recent studies suggested that it may also be associated with peripheral nerve injury. It was reported

that mRNA level of MAOB was upregulated in sciatic nerve of rats after chronic constriction injury (Stevens et al., 2019). Inhibition of MAOB can upregulate myelin basic protein expression and promote axon regeneration in the sciatic nerve injury model of rats (Hussain et al., 2018). Inhibition of MAOB also alleviated the pain effect in mouse models of acute postoperative pain and chronic neuropathic pain (Villarinho et al., 2012). In our work, we firstly found that MAOB not MAOA is selectively overexpressed in spinal cord and DRG tissues of PIPN mice, and Khe as a selective MAOB inhibitor efficiently ameliorated neurological dysfunctions in PIPN mice. Given the important role of MAOB in peripheral neuropathy, it is expected to be a promising target for the treatment of PIPN.

PTX was reported to be easily invaded and accumulated in DRG tissues (Scripture et al., 2006) and PTX is also detectable in spinal cord presumably owing to its transportation through the centrifugal and centripetal branches of DRG neuronal axons (Leblanc et al., 2018), which caused neuronal apoptosis and axonal degeneration (Huang et al., 2014). In our work, we also detected PTX level in the spinal cord tissue at different time points after construction of PIPN model (PTX was intraperitoneally injected to male C57BL/6N mice at a dose of 4 mg/kg on day 0, 2, 4, and 6 with a final cumulative dose of 16 mg/kg.) and found that it was detectable (Fig. S5). In addition, PTX affected mitochondria in the neurons by opening mitochondrial permeability transition pores and increasing ROS production (Bernardi et al., 2006), resulting in axon degeneration and neuronal apoptosis (Canta et al., 2015). Here, we demonstrated that Khe as a selective MAOB inhibitor effectively enhanced neurite

outgrowth, ameliorated mitochondrial dysfunction of DRG neurons, and protected against DRG neuronal apoptosis in PIPN mice.

It is well known that astrocytes and microglia in SCDH produce pro-inflammatory mediators including TNF-α and IL-1β, which are important contributors to PIPN pathology (Luo et al., 2019; Yan et al., 2019). In addition, PIPN model rats also showed significant activation of both microglia and astrocytes in SCDH (Li et al., 2021). However, we here determined that PIPN mice significantly showed activation of astrocyte not microglia in SCDH, and Khe treatment inhibited this activation in PIPN mice. This discrepancy might be due to the fact that microglia are significantly activated at an early time point after PTX treatment (Zhang et al., 2012). Moreover, PTX elicits mitochondria damage and ROS production resulting in activation of NLRP3 inflammasome, which contributes to PTX-induced neuropathic pain (Jia et al., 2017). Our results have indicated that Khe treatment suppressed neuroinflammation of spinal cord via MAOB/NF-κB/NLRP3/ASC/Caspase1/IL-1β pathway in PIPN mice, demonstrating the potential mechanism underlying the regulation of MAOB against neuroinflammation in PIPN pathology with Khe as a probe.

Additionally, we also investigated whether Khe had impacts on the antitumor activity of PTX. Normal cell apoptosis can maintain the renewal and stability of tissues. Tumor cells circumvent apoptosis by inhibiting TP53 tumor suppressor function, regulating expression of antiapoptotic (Bcl-2, Bcl-xL) or proapoptotic factors (Bax, Bim, Puma) and short-circuiting the extrinsic ligand-induced death

pathway (Hanahan and Weinberg, 2011), which is one of the hallmarks of cancer. However, PTX exerted its anti-tumor effect by inhibiting mitosis and inducing apoptosis. In consideration of clinical use, human breast cancer cells MCF7 were selected to evaluate the effect of Khe on the anti-tumor efficiency of PTX. The result showed that Khe did not reduce the chemotherapeutic efficacy of PTX *in vitro* or *in vivo*. Since we aimed to explore the neuroprotective effect of Khe, the relationship between Khe and cancer cells was not thoroughly studied. To fully understand the effects of Khe on tumor cells, long-term anti-tumor studies are still needed.

In summary, our study indicated that MAOB not MAOA is highly overexpressed in spinal cord and DRG tissues of PIPN mice, and herbal folk medicine Khe as a selective MAOB inhibitor efficiently ameliorated neurological dysfunctions in PIPN mice. The underlying mechanisms have been intensively investigated. As illustrated in Fig. 11, Khe improved mitochondrial dysfunction of DRG neurons and further alleviated apoptosis by regulation of apoptosis-related protein such as Bcl-2, Bax and C-caspase3 in PIPN mice by targeting MAOB. In addition, Khe also inhibited spinal astrocytes activation and suppressed neuroinflammation of spinal astrocytes in PIPN mice via MAOB/NF-κB/NLRP3/ASC/Caspase1/IL-1β pathway. Collectively, our findings have highly addressed the potency of selective MAOB inhibitor in the amelioration of PIPN-like pathology and highlighted the potential of Khe in treating PTX-induced side effect.

CRediT authors contribution statement

Xingnan Ouyang: Conceptualization, Methodology, Validation, Formal analysis, Investigation, Writing-Original Draft. **Danyang Zhu:** Validation, Formal analysis, Investigation, Writing-Review & Editing. **Yujie Huang:** Formal analysis, Investigation, Resources, Data Curation. **Rui Xu:** Resources, Data Curation. **Wenjun Li:** Formal analysis, Investigation, Data Curation, Writing-Review & Editing. **Jiaying Wang:** Formal analysis, Data Curation, Writing-Review & Editing, Funding acquisition. **Xu Shen:** Conceptualization, Investigation, Data Curation, Writing-Review & Editing, Project administration, Funding acquisition. All data were generated in-house, and no paper mill was used. All authors agree to be accountable for all aspects of work ensuring integrity and accuracy.

Data availability

The data sets supporting the conclusions of this article are available from the corresponding author, on reasonable request.

Funding

This work was supported by the National Natural Science Foundation of China (82273930), Innovative Research Team of Six Talent Peaks Project in Jiangsu Province (TD-SWYY-013), the National Natural Science Foundation for Young Scientists of China (82204486), the Open Project of Chinese Materia Medica First-Class Discipline of Nanjing University of Chinese Medicine (2020YLXK018) “Qing Lan” project, and Natural Science Foundation of Jiangsu Province (BK20200570).

Declaration of Competing Interest

The authors declare that they have no known competing financial interests or personal relationships that could have appeared to influence the work reported in this paper.

References

Ambrosini, G., Do, C., Tycko, B., Realubit, R.B., Karan, C., Musi, E., Carvajal, R.D., Chua, V., Aplin, A.E., Schwartz, G.K., 2019. Inhibition of NF-kappaB-dependent signaling enhances sensitivity and overcomes resistance to BET inhibition in uveal melanoma. Cancer Res 79, 2415-2425.

Amira Mohammed Beltagy, D.M.B., 2015. Chemical composition of Ammi visnaga L. and new cytotoxic activity of its constituents Khellin and Visnagin. J PHARM SCI-US 7, 285-291.

Bar-Am, O., Amit, T., Kupershmidt, L., Aluf, Y., Mechlovich, D., Kabha, H., Danovitch, L., Zurawski, V.R., Youdim, M.B., Weinreb, O., 2015. Neuroprotective and neurorestorative activities of a novel iron chelator-brain selective monoamine oxidase-A/monoamine oxidase-B inhibitor in animal models of Parkinson's disease and aging. Neurobiol Aging 36, 1529-1542.

Bernardi, P., Krauskopf, A., Basso, E., Petronilli, V., Blachly-Dyson, E., Di Lisa, F., Forte, M.A., 2006. The mitochondrial permeability transition from in vitro artifact to disease target. FEBS J 273, 2077-2099.

Burch, R., 2019. Antidepressants for preventive treatment of migraine. Curr Treat Options Neurol 21, 18-30.

Canta, A., Pozzi, E., Carozzi, V.A., 2015. Mitochondrial dysfunction in chemotherapy-induced peripheral neuropathy (CIPN). Toxics 3, 198-223.

Chen, T., Hu, W., He, H.B., Gong, Z.P., Wang, J., Yu, X.Q., Ai, T., Zhan, L., 2013. A study on the mechanism of cinobufagin in the treatment of paw cancer pain by modulating local beta-endorphin expression in vivo. Evid-Based Compl Alt 2013, 851256-851265.

Chine, V.B., Au, N.P.B., Kumar, G., Ma, C.H.E., 2019. Targeting axon integrity to prevent chemotherapy-induced peripheral neuropathy. Mol Neurobiol 56, 3244-3259.

Chistiakov, D.A., Killingsworth, M.C., Myasoedova, V.A., Orekhov, A.N., Bobryshev, Y.V., 2017. CD68/macrosialin: not just a histochemical marker. Lab Invest 97, 4-13.

Chun, H., Im, H., Kang, Y.J., Kim, Y., Shin, J.H., Won, W., Lim, J., Ju, Y., Park, Y.M., Kim, S., Lee, S.E., Lee, J., Woo, J., Hwang, Y., Cho, H., Jo, S., Park, J.H., Kim, D., Kim, D.Y., Seo, J.S., Gwag, B.J., Kim, Y.S., Park, K.D., Kaang, B.K., Cho, H., Ryu, H., Lee, C.J., 2020. Severe reactive astrocytes precipitate pathological hallmarks of Alzheimer's disease via H_2O_2- production. Nat Neurosci 23, 1555-1542.

Duggett, N.A., Griffiths, L.A., Flatters, S.J.L., 2017. Paclitaxel-induced painful neuropathy is associated with changes in mitochondrial bioenergetics, glycolysis, and an energy deficit in dorsal root ganglia neurons. Pain 158, 1499-1508.

Hanahan, D., Weinberg, R.A., 2011. Hallmarks of cancer: the next generation. Cell 144, 646-674.

Hu, L.Y., Mi, W.L., Wu, G.C., Wang, Y.Q., Mao-Ying, Q.L., 2019. Prevention and

treatment for chemotherapy-induced peripheral neuropathy: Therapies based on CIPN mechanisms. Curr Neuropharmacol 17, 184-196.

Huang, Z.Z., Li, D., Liu, C.C., Cui, Y., Zhu, H.Q., Zhang, W.W., Li, Y.Y., Xin, W.J., 2014. CX3CL1-mediated macrophage activation contributed to paclitaxel-induced DRG neuronal apoptosis and painful peripheral neuropathy. Brain Behav Immun 40, 155-165.

Hussain, A.S.M., Renno, W.M., Sadek, H.L., Kayali, N.M., Al-Salem, A., Rao, M.S., Khan, K.M., 2018. Monoamine oxidase-B inhibitor protects degenerating spinal neurons, enhances nerve regeneration and functional recovery in sciatic nerve crush injury model. Neuropharmacology 128, 231-243.

Jhaveri, D.J., Tedoldi, A., Hunt, S., Sullivan, R., Watts, N.R., Power, J.M., Bartlett, P.F., Sah, P., 2018. Evidence for newly generated interneurons in the basolateral amygdala of adult mice. Mol Psychiatry 23, 521-532.

Jia, M., Wu, C., Gao, F., Xiang, H., Sun, N., Peng, P., Li, J., Yuan, X., Li, H., Meng, X., Tian, B., Shi, J., Li, M., 2017. Activation of NLRP3 inflammasome in peripheral nerve contributes to paclitaxel-induced neuropathic pain. Mol Pain 13, 1-11.

Kanbayashi, Y., Inagaki, M., Ueno, H., Hosokawa, T., 2017. Predictors of the usefulness of duloxetine for chemotherapy-induced peripheral neuropathy. Med Oncol 34, 137-142.

Kautio, A.L., Haanpaa, M., Saarto, T., Kalso, E., 2008. Amitriptyline in the treatment of chemotherapy-induced neuropathic symptoms. J Pain Symptom Manag 35,

31-39.

Kirchmair, R., Tietz, A.B., Panagiotou, E., Walter, D.H., Silver, M., Yoon, Y.S., Schratzberger, P., Weber, A., Kusano, K., Weinberg, D.H., Ropper, A.H., Isner, J.M., Losordo, D.W., 2007. Therapeutic angiogenesis inhibits or rescues chemotherapy-induced peripheral neuropathy: taxol- and thalidomide-induced injury of vasa nervorum is ameliorated by VEGF. Mol Ther 15, 69-75.

Leblanc, A.F., Sprowl, J.A., Alberti, P., Chiorazzi, A., Arnold, W.D., Gibson, A.A., Hong, K.W., Pioso, M.S., Chen, M., Huang, K.M., Chodisetty, V., Costa, O., Florea, T., de Bruijn, P., Mathijssen, R.H., Reinbolt, R.E., Lustberg, M.B., Sucheston-Campbell, L.E., Cavaletti, G., Sparreboom, A., Hu, S., 2018. OATP1B2 deficiency protects against paclitaxel-induced neurotoxicity. J Clin Invest 128, 816-825.

Li, Y.Y., Yin, C.Y., Liu, B.Y., Nie, H.M., Wang, J., Zeng, D.Y., Chen, R.X., He, X.F., Fang, J.F., Du, J.Y., Liang, Y., Jiang, Y.L., Fang, J.Q., Liu, B.Y., 2021. Transcriptome profiling of long noncoding RNAs and mRNAs in spinal cord of a rat model of paclitaxel-induced peripheral neuropathy identifies potential mechanisms mediating neuroinflammation and pain. J Neuroinflamm 18, 48-70.

Li, Z., Mao, Y., Liang, L., Wu, S., Yuan, J., Mo, K., Cai, W., Mao, Q., Cao, J., Bekker, A., Zhang, W., Tao, Y.X., 2017. The transcription factor C/EBPbeta in the dorsal root ganglion contributes to peripheral nerve trauma-induced nociceptive hypersensitivity. Sci Signal 10, 1-29.

Liu, M., Zhang, S.B., Luo, Y.X., Yang, Y.L., Zhang, X.Z., Li, B., Meng, Y., Chen, Y.J.,

Guo, R.X., Xiong, Y.C., Xin, W.J., Li, D., 2020. NFATc2-dependent epigenetic upregulation of CXCL14 is involved in the development of neuropathic pain induced by paclitaxel. J Neuroinflamm 17, 310-322.

Liu, X., Tonello, R., Ling, Y., Gao, Y.J., Berta, T., 2019. Paclitaxel-activated astrocytes produce mechanical allodynia in mice by releasing tumor necrosis factor-alpha and stromal-derived cell factor 1. J Neuroinflamm 16, 209-223.

Lu, Y., Zhang, P., Zhang, Q., Yang, C., Qian, Y., Suo, J., Tao, X., Zhu, J., 2020. Duloxetine attenuates paclitaxel-induced peripheral nerve injury by inhibiting p53-related pathways. J Pharmacol Exp Ther 373, 453-462.

Luo, H., Liu, H.Z., Zhang, W.W., Matsuda, M., Lv, N., Chen, G., Xu, Z.Z., Zhang, Y.Q., 2019. Interleukin-17 regulates neuron-glial communications, synaptic transmission, and neuropathic pain after chemotherapy. Cell Rep 29, 2384-2397.

Meng, J., Zhang, Q., Yang, C., Xiao, L., Xue, Z., Zhu, J., 2019. Duloxetine, a balanced serotonin-norepinephrine reuptake inhibitor, improves painful chemotherapy-induced peripheral neuropathy by inhibiting activation of p38 MAPK and NF-kappaB. Front Pharmacol 10, 365-380.

Milligan, E.D., Watkins, L.R., 2009. Pathological and protective roles of glia in chronic pain. Nat Rev Neurosci 10, 23-36.

Morioka, N., Kodama, K., Tomori, M., Yoshikawa, K., Saeki, M., Nakamura, Y., Zhang, F.F., Hisaoka-Nakashima, K., Nakata, Y., 2019. Stimulation of nuclear receptor REV-ERBs suppresses production of pronociceptive molecules in cultured spinal astrocytes and ameliorates mechanical hypersensitivity of

inflammatory and neuropathic pain of mice. Brain Behav Immun 78, 116-130.

Ng, K.P., Pascoal, T.A., Mathotaarachchi, S., Therriault, J., Kang, M.S., Shin, M., Guiot, M.C., Guo, Q., Harada, R., Comley, R.A., Massarweh, G., Soucy, J.P., Okamura, N., Gauthier, S., Rosa-Neto, P., 2017. Monoamine oxidase B inhibitor, selegiline, reduces (18)F-THK5351 uptake in the human brain. Alzheimers Res Ther 9, 25-34.

Nie, B., Liu, C., Bai, X., Chen, X., Wu, S., Zhang, S., Huang, Z., Xie, M., Xu, T., Xin, W., Zeng, W., Ouyang, H., 2018. AKAP150 involved in paclitaxel-induced neuropathic pain via inhibiting CN/NFAT2 pathway and downregulating IL-4. Brain Behav Immun 68, 158-168.

Pease-Raissi, S.E., Pazyra-Murphy, M.F., Li, Y., Wachter, F., Fukuda, Y., Fenstermacher, S.J., Barclay, L.A., Bird, G.H., Walensky, L.D., Segal, R.A., 2017. Paclitaxel reduces axonal Bclw to initiate IP3R1-dependent axon degeneration. Neuron 96, 373-386.

Peters, C.M., Jimenez-Andrade, J.M., Jonas, B.M., Sevcik, M.A., Koewler, N.J., Ghilardi, J.R., Wong, G.Y., Mantyh, P.W., 2007. Intravenous paclitaxel administration in the rat induces a peripheral sensory neuropathy characterized by macrophage infiltration and injury to sensory neurons and their supporting cells. Exp Neurol 203, 42-54.

Sanchez-Rodriguez, R., Munari, F., Angioni, R., Venegas, F., Agnellini, A., Castro-Gil, M.P., Castegna, A., Luisetto, R., Viola, A., Canton, M., 2021. Targeting monoamine oxidase to dampen NLRP3 inflammasome activation in

inflammation. Cell Mol Immunol 18, 1311-1313.

Scripture, C.D., Figg, W.D., Sparreboom, A., 2006. Peripheral neuropathy induced by paclitaxel: recent insights and future perspectives. Curr Neuropharmacol 4, 165-172.

Sekiguchi, F., Domoto, R., Nakashima, K., Yamasoba, D., Yamanishi, H., Tsubota, M., Wake, H., Nishibori, M., Kawabata, A., 2018. Paclitaxel-induced HMGB1 release from macrophages and its implication for peripheral neuropathy in mice: Evidence for a neuroimmune crosstalk. Neuropharmacology 141, 201-213.

Shulman, K.I., Herrmann, N., Walker, S.E., 2013. Current place of monoamine oxidase inhibitors in the treatment of depression. CNS Drugs 27, 789-797.

Singhmar, P., Huo, X.J., Li, Y., Dougherty, P.M., Mei, F., Cheng, X.D., Heijnen, C.J., Kavelaars, A., 2018. Orally active Epac inhibitor reverses mechanical allodynia and loss of intraepidermal nerve fibers in a mouse model of chemotherapy-induced peripheral neuropathy. Pain 159, 884-893.

Sivenius, J., Sarasoja, T., Aaltonen, H., Heinonen, E., Kilkku, O., Reinikainen, K., 2001. Selegiline treatment facilitates recovery after stroke. Neurorehabil Neural Repair 15, 183-190.

Son, S., Shim, D.W., Hwang, I., Park, J.H., Yu, J.W., 2019. Chemotherapeutic agent paclitaxel mediates priming of NLRP3 inflammasome activation. Front Immunol 10, 1108-1118.

Sorato, E., Menazza, S., Zulian, A., Sabatelli, P., Gualandi, F., Merlini, L., Bonaldo, P., Canton, M., Bernardi, P., Di Lisa, F., 2014. Monoamine oxidase inhibition

prevents mitochondrial dysfunction and apoptosis in myoblasts from patients with collagen VI myopathies. Free Radic Biol Med 75, 40-47.

Stevens, A.M., Liu, L., Bertovich, D., Janjic, J.M., Pollock, J.A., 2019. Differential expression of neuroinflammatory mRNAs in the rat sciatic nerve following chronic constriction injury and pain-relieving nanoemulsion NSAID delivery to infiltrating macrophages. Int J Mol Sci 20, 5269-5293.

Umbarkar, P., Singh, S., Arkat, S., Bodhankar, S.L., Lohidasan, S., Sitasawad, S.L., 2015. Monoamine oxidase-A is an important source of oxidative stress and promotes cardiac dysfunction, apoptosis, and fibrosis in diabetic cardiomyopathy. Free Radical Bio Med 87, 263-273.

Usmani, Q.I., Jahan, N., Aleem, M., Hasan, S.A., 2021. Aatrilal (Ammi majus L.), an important drug of Unani system of medicine: A review. J Ethnopharmacol 276, 114144-114158.

Villarinho, J.G., Oliveira, S.M., Silva, C.R., Cabreira, T.N., Ferreira, J., 2012. Involvement of monoamine oxidase B on models of postoperative and neuropathic pain in mice. Eur J Pharmacol 690, 107-114.

Vrzal, R., Frauenstein, K., Proksch, P., Abel, J., Dvorak, Z., Haarmann-Stemmann, T., 2013. Khellin and Visnagin differentially modulate AHR signaling and downstream CYP1A activity in human liver cells. Plos One 8, e74917.

Yan, X.S., Li, F., Maixner, D.W., Yadav, R., Gao, M., Ali, M.W., Hooks, S.B., Weng, H.R., 2019. Interleukin-1beta released by microglia initiates the enhanced glutamatergic activity in the spinal dorsal horn during paclitaxel-associated acute

pain syndrome. Glia 67, 482-497.

Yang, Y., Wen, J., Zheng, B., Wu, S., Mao, Q., Liang, L., Li, Z., Bachmann, T., Bekker, A., Tao, Y.X., 2021. CREB participates in paclitaxel-induced neuropathic pain genesis through transcriptional activation of Dnmt3a in primary sensory neurons. Neurotherapeutics 18, 586-600.

Zhang, H., Yoon, S.Y., Zhang, H., Dougherty, P.M., 2012. Evidence that spinal astrocytes but not microglia contribute to the pathogenesis of Paclitaxel-induced painful neuropathy. J Pain 13, 293-303.

Zhu, X., Chen, Y., Xu, X., Xu, X., Lu, Y., Huang, X., Zhou, J., Hu, L., Wang, J., Shen, X., 2020. SP6616 as a Kv2.1 inhibitor efficiently ameliorates peripheral neuropathy in diabetic mice. EBioMedicine 61, 103061-103077.

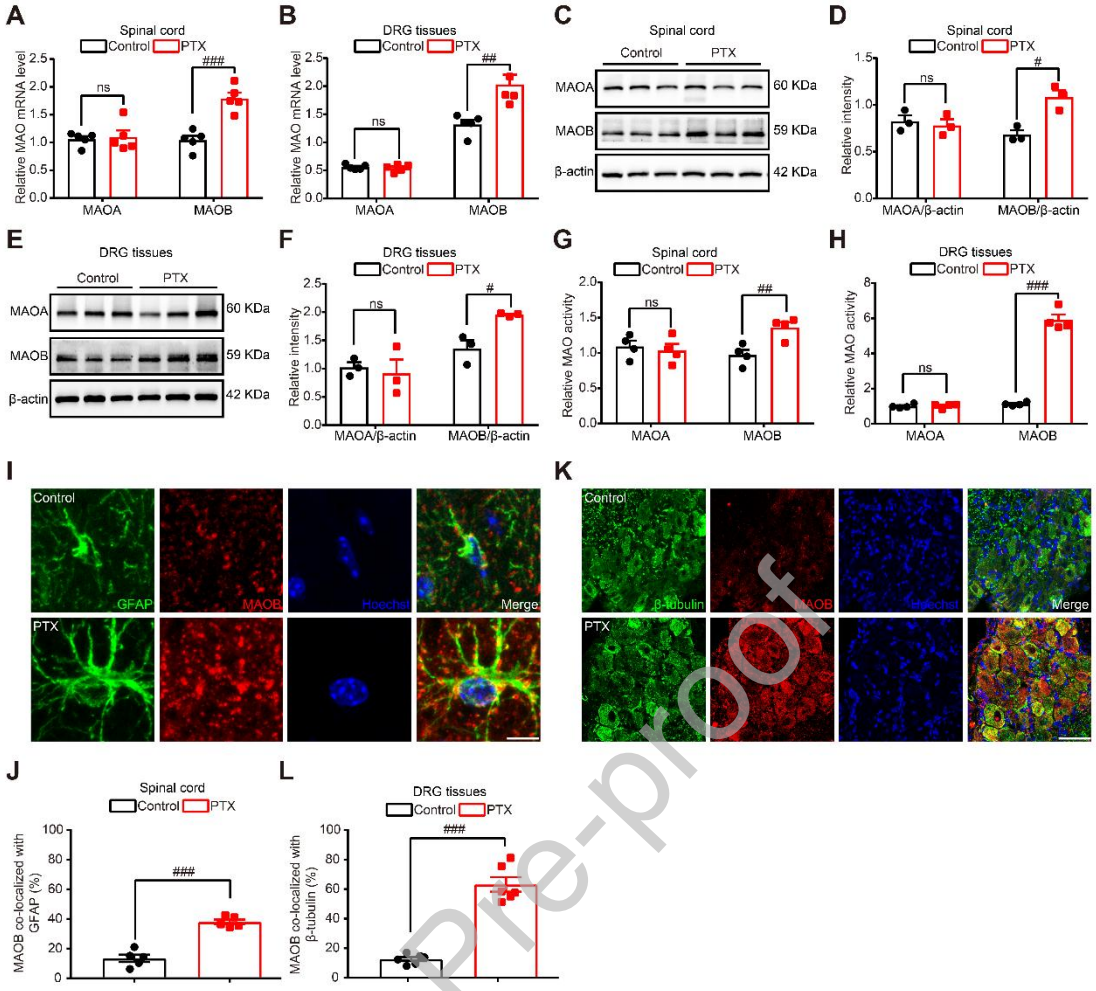

Fig. 1 MAOB was selectively overexpressed in spinal astrocytes and neurons of DRG tissues of PIPN mice. qRT-PCR results demonstrated that mRNA level of MAOB not MAOA was upregulated in **(A)** spinal cord or **(B)** DRG tissues of PIPN mice (n = 5). Western blot with quantification results indicated that the protein expressions of MAOB not MAOA were upregulated in **(C, D)** spinal cord and **(E, F)** DRG tissues of PIPN mice (n = 3). The result by commercial MAOs enzymatic detection kit indicated that the enzymatic activity of MAOB not MAOA was upregulated in **(G)** spinal cord and **(H)** DRG tissues of PIPN mice (n = 4). **(I, J)** Immunofluorescence with quantification results demonstrated that MAOB (red) was colocalized primarily with astrocytes (as indicated by GAFP, astrocytic marker, green)

in SCDH (n = 5). Scale bar: 5 μm. **(K, L)** Immunofluorescence with quantification results demonstrated that MAOB (red) was colocalized primarily with neurons (as indicated by β-tubulin III, neuronal marker, green) in DRG tissues (n = 6). Scale bar: 25 μm. β-actin was used as loading control in western blot assays. All values were presented as mean ± SEM. $^{\#}p < 0.05$, $^{\#\#}p < 0.01$, $^{\#\#\#}p < 0.001$ compared with Control group by Student's t test.

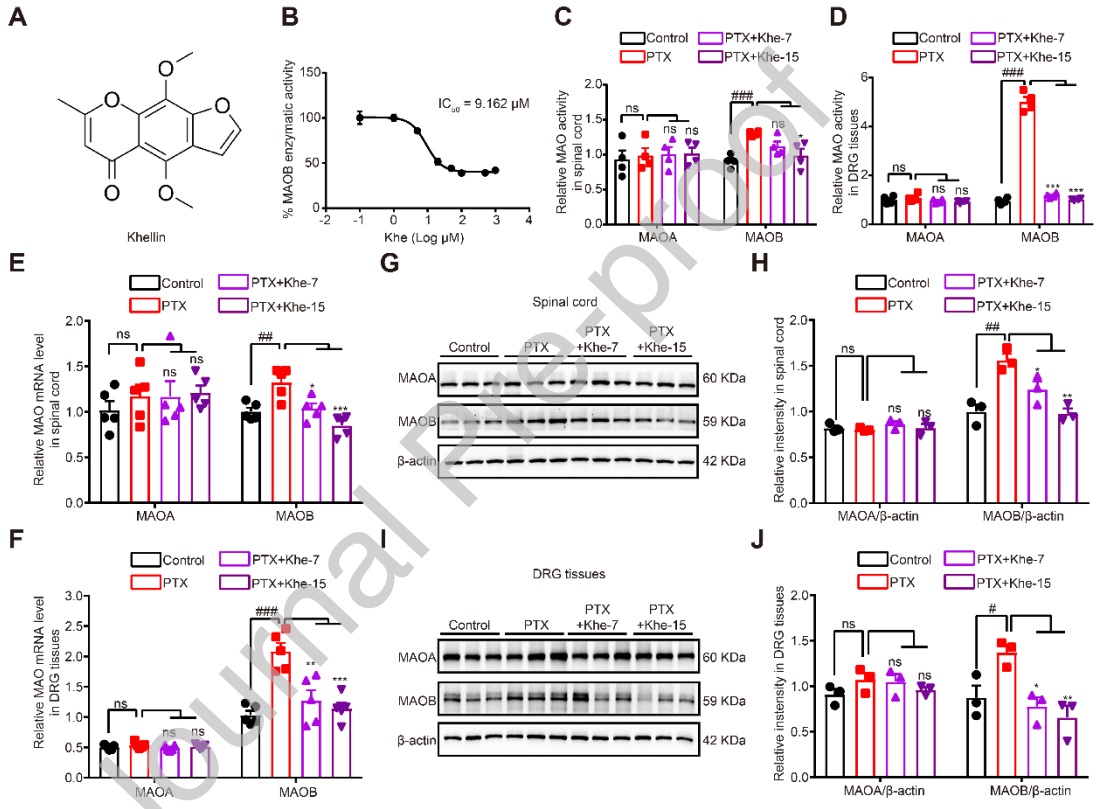

Fig. 2 Khe was a MAOB selective inhibitor. (A) Chemical structure of Khe. **(B)** Khe inhibited MAOB activity by IC_{50} at 9.162 μM. Khe (7, 15 mg/kg/day) treatment inhibited the enzymatic activity of MAOB not MAOA in **(C)** spinal cord and **(D)** DRG tissues of PIPN mice (n = 4). qRT-PCR results indicated that Khe (7, 15 mg/kg/day) treatment inhibited the mRNA levels of MAOB not MAOA in **(E)** spinal cord and **(F)** DRG tissues of PIPN mice (n = 5). Western blot with quantification

results demonstrated that Khe (7, 15 mg/kg/day) treatment downregulated the expressions of MAOB not MAOA in **(G, H)** spinal cord and **(I, J)** DRG tissues of PIPN mice (n = 3). β-actin was used as loading control in western blot assays. All values were presented as mean ± SEM. $^{\#}p < 0.05$, $^{\#\#}p < 0.01$, $^{\#\#\#}p < 0.001$ compared with Control group by Student's t test. $^{*}p < 0.05$, $^{**}p < 0.01$, $^{***}p < 0.001$ compared with PTX group by One-way ANOVA with Dunnett's post-hoc test. $F_{(2, 9)} = 5.18$ **(C)**, $F_{(2, 9)} = 359.7$ **(D)**, $F_{(2, 12)} = 15.5$ **(E)**, $F_{(2, 6)} = 15.7$ **(H)**, $F_{(2, 12)} = 13.5$ **(F)**, $F_{(2, 6)} = 12.92$ **(J).**

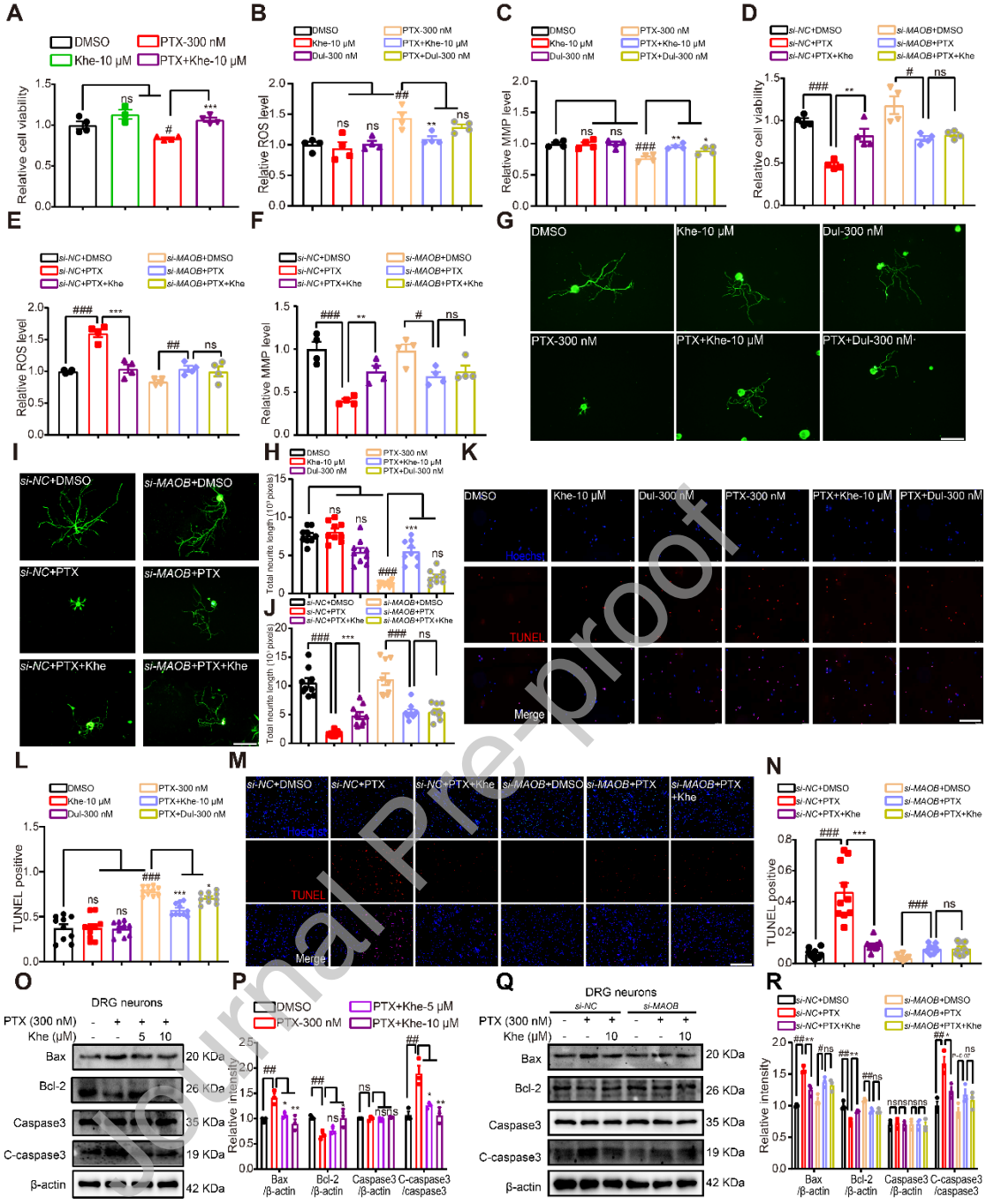

Fig. 3 Khe protected DRG neurons from PTX-induced damage by targeting MAOB. (A) MTT assay results indicated that Khe (10 μM) protected primary DRG neurons from PTX (300 nM)-induced neurotoxicity (n = 4). Khe antagonized the PTX-induced **(B)** ROS upregulation and **(C)** MMP downregulation in primary DRG neurons, whereas Dul was less effective compared with Khe (n = 4). *si-MAOB* deprived Khe of its effects on **(D)** cell viability, **(E)** ROS or **(F)** MMP levels in

PTX-treated primary DRG neurons (n = 4). Immunofluorescence (β-tubulin III labelled DRG neurons, green) with quantification results demonstrated that **(G, H)** Khe antagonized PTX-induced inhibition against the neurite outgrowth of DRG neurons, while Dul had no significant effect on neurite outgrowth. **(I, J)** *si-MAOB* deprived Khe of its above-mentioned antagonistic capability in PTX-treated primary DRG neurons (n = 9). Scale bar: 50 μm. TUNEL assay with quantification results demonstrated that **(K, L)** Khe and Dul antagonized PTX-induced apoptosis and **(M, N)** *si-MAOB* deprived Khe of its anti-apoptotic capability in PTX-treated primary DRG neurons (n = 10). Scale bar: 75 μm. Western blot with quantification results showed that **(O, P)** Khe (5, 10 μM) antagonized the PTX-induced downregulation of anti-apoptotic protein Bcl-2 and upregulation of pro-apoptotic proteins Bax and C-caspase3, while **(Q, R)** *si-MAOB* deprived Khe of its anti-apoptotic capability in PTX-treated primary DRG neurons (n = 3). β-actin was used as loading control in western blot assays. All values were presented as mean ± SEM. $^{\#}p < 0.05$, $^{\#\#}p < 0.01$, $^{\#\#\#}p < 0.001$ compared with DMSO group by Student's t test. $^{*}p < 0.05$, $^{**}p < 0.01$, $^{***}p < 0.001$ compared with PTX group by One-way ANOVA with Dunnett's post-hoc test. $F_{(2, 9)} = 7.171$ **(B)**, $F_{(2, 9)} = 11.95$ **(C)**, $F_{(2, 24)} = 42.31$ **(H)**, $F_{(2, 27)} = 29.33$ **(L)**, $F_{(2, 6)} = 14.40$ for Bax **(P)**, $F_{(2, 6)} = 5.845$ for Bcl-2 **(P)**, $F_{(2, 6)} = 0.4752$ for Casspase3 **(P)**, $F_{(2, 6)} = 16.92$ for C-caspase3 **(P)**.

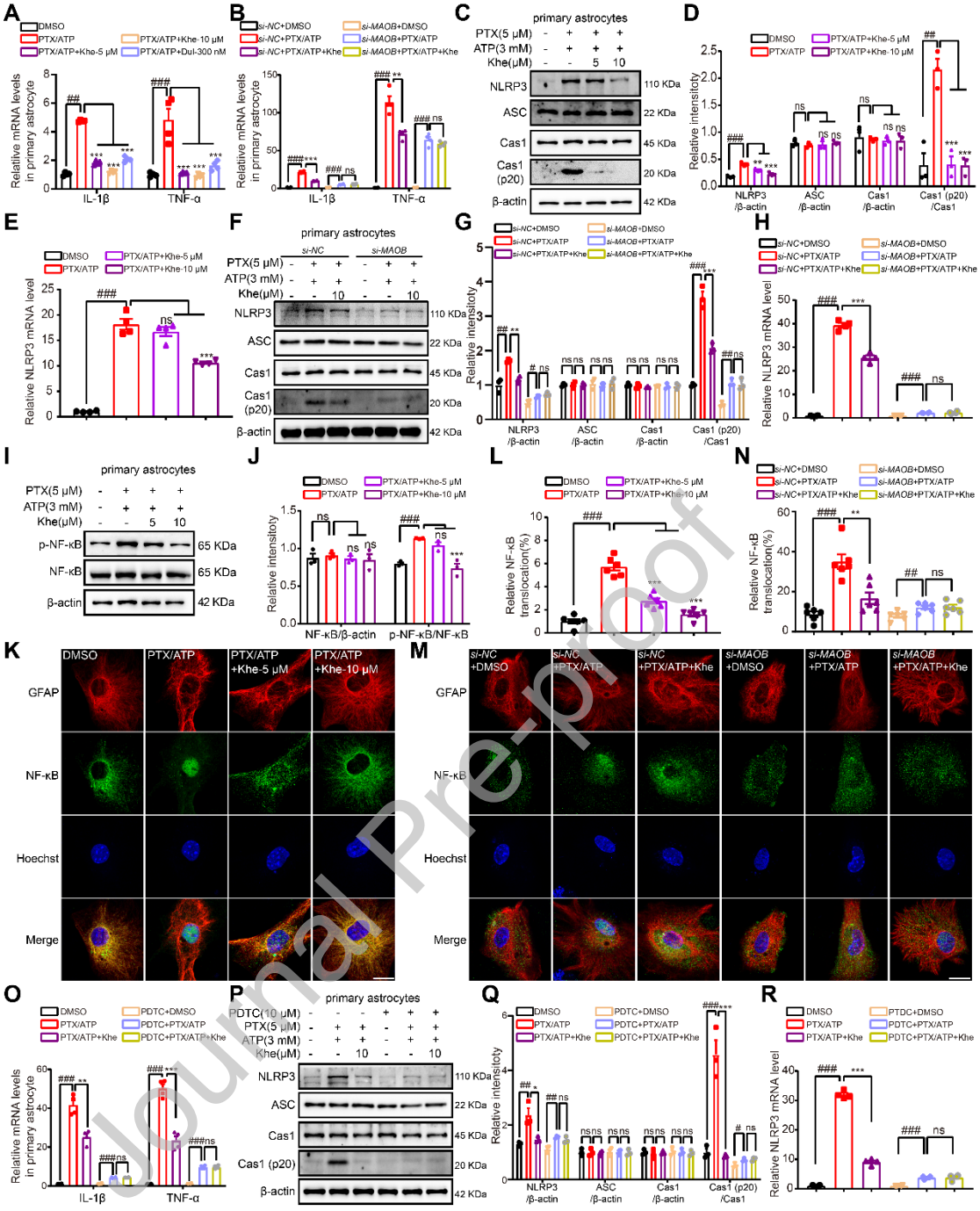

Fig. 4 Khe suppressed neuroinflammation in PTX/ATP-treated primary astrocytes through MAOB/NF-κB/NLRP3/ASC/Caspase1/IL-1β pathway. qRT-PCR results indicated that **(A)** Khe (5, 10 μM) and Dul antagonized PTX/ATP-induced upregulation of the mRNA levels of IL-1β and TNF-α, while **(B)** *si-MAOB* deprived Khe of its antagonistic capabilities in PTX/ATP-treated primary astrocytes (n = 4). Western blot with quantification results demonstrated that **(C, D)**

Khe antagonized the PTX/ATP-induced upregulation of protein levels of NLRP3 and Cas1 (p20), while **(F, G)** *si-MAOB* deprived Khe of its above antagonistic capability in PTX/ATP-treated primary astrocytes (n = 3). qRT-PCR results showed that **(E)** Khe antagonized the PTX/ATP-induced upregulation of mRNA level of NLRP3, while **(H)** *si-MAOB* deprived Khe of its antagonistic capability in PTX/ATP-treated primary astrocytes (n = 4). **(I, J)** Western blot with quantification results indicated that Khe antagonized PTX/ATP-induced upregulation of the protein levels of NF-κB and p-NF-κB in PTX/ATP-treated primary astrocytes (n = 3). Immunofluorescence with quantification results demonstrated that **(K, L)** Khe antagonized PTX/ATP-induced promotion of NF-κB nuclear translocation and **(M, N)** *si-MAOB* deprived Khe of its antagonistic capability in PTX/ATP-treated primary astrocytes (n = 6). Scale bar: 5 μm. **(O)** qRT-PCR results showed that PDTC deprived Khe of its suppressive capability against IL-1β and TNF-α in PTX/ATP-treated primary astrocytes (n = 4). **(P, Q)** Western blot with quantification results showed that PDTC deprived Khe of its suppressive capability against NLRP3 and Cas1 (p20) in PTX/ATP-treated primary astrocytes (n = 3). **(R)** qRT-PCR results showed that PDTC deprived Khe of its suppressive capability against NLRP3 in PTX/ATP-treated primary astrocytes (n = 4). β-actin was used as loading control in western blot assays. All values were presented as mean ± SEM. $^{\#}p < 0.05$, $^{\#\#}p < 0.01$, $^{\#\#\#}p < 0.001$ compared with DMSO group by Student's t test. $^{*}p < 0.05$, $^{**}p < 0.01$, $^{***}p < 0.001$ compared with PTX/ATP group by One-way ANOVA with Dunnett's post-hoc test. $F_{(3, 12)} = 601.0$ for IL-1β **(A)**, $F_{(3, 12)} = 21.09$ for TNF-α **(A)**, $F_{(2, 6)} = 32.4$ for NLRP3 **(D)**, $F_{(2, 6)} = 0.2679$ for ASC **(D)**, F

$_{(2, 6)}$ = 0.05632 for Cas1 **(D)**, $F_{(2, 6)}$ = 44.5 for Cas1 (p20) **(D)**, $F_{(2, 9)}$ = 24.6 **(E)**, $F_{(2, 6)}$ = 0.0239 for NF-κB **(J)**, $F_{(2, 6)}$ = 23.9 for p-NF-κB **(J)**, $F_{(2, 15)}$ = 68.66 **(L)**.

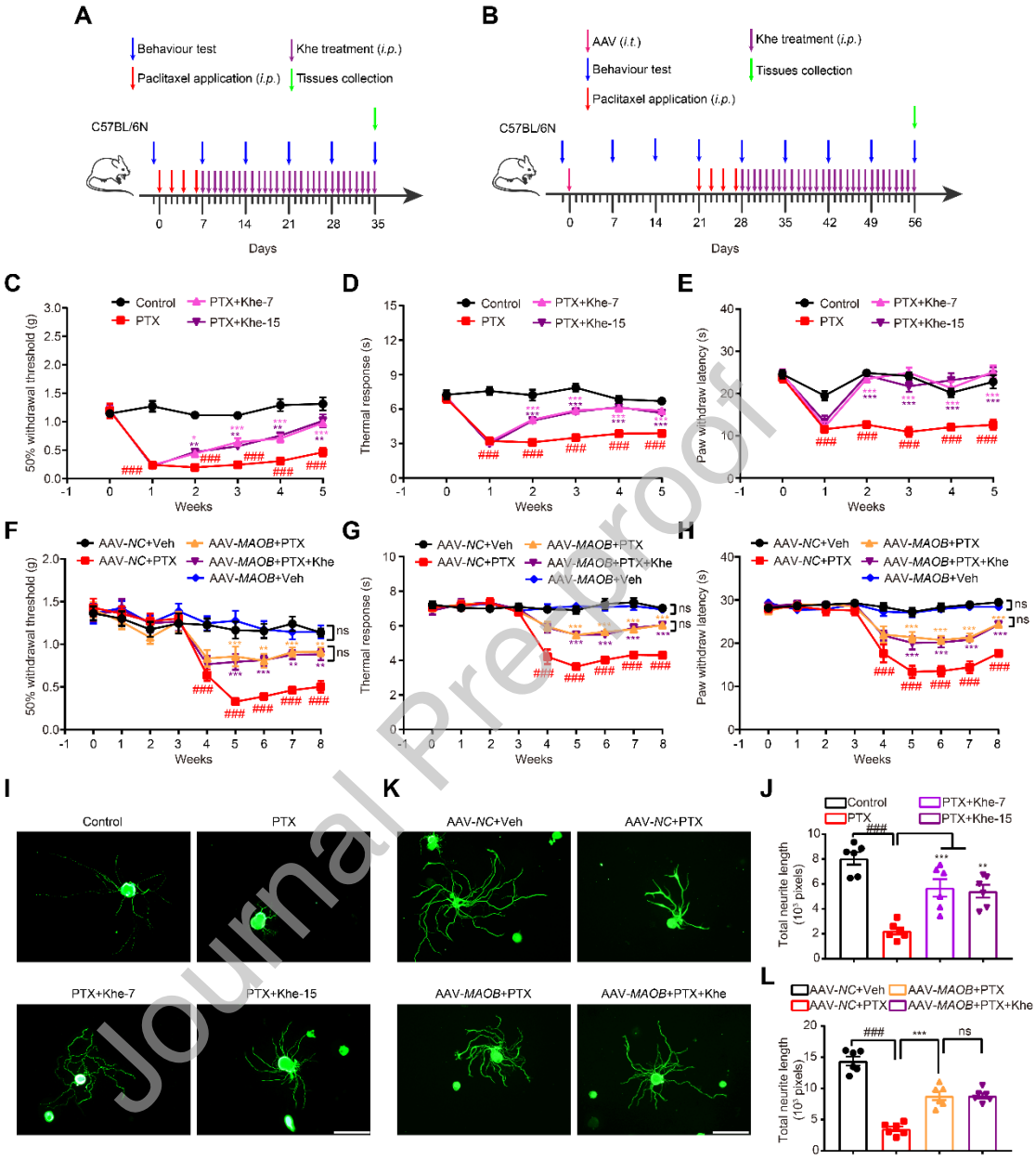

Fig. 5 Khe ameliorated neurological dysfunctions and enhanced DRG neurite outgrowth in PIPN mice by targeting MAOB. Schedule of animal treatment and behavior test for **(A)** PIPN mice and **(B)** AAV-*MAOB-shRNA*-injected PIPN mice. Behavior test results showed that Khe (7, 15 mg/kg/day) treatment or AAV-*MAOB-shRNA* injection ameliorated **(C, F)** 50% mechanical threshold, **(D, G)**

thermal response latency and **(E, H)** paw withdrawal responses to cold stimulate in PIPN mice (n = 10), and **(F-H)** Khe (15 mg/kg/day) treatment had no impacts on neurological dysfunctions in AAV-*MAOB-shRNA* injected PIPN mice (n = 12). Immunofluorescence (β-tubulin III labelled DRG neurons, green) with quantification results demonstrated that **(I, J)** Khe (7, 15 mg/kg/day) treatment or **(K, L)** AAV-*MAOB-shRNA* injection enhanced the neurite outgrowth of DRG neurons from PIPN mice, and **(K, L)** Khe (15 mg/kg/day) treatment had no impacts on neurite outgrowth of DRG neurons from AAV-*MAOB-shRNA* injected PIPN mice (n = 6). Scale bar: 50 μm. All values were presented as mean ± SEM. $^{\#}p < 0.05$, $^{\#\#}p < 0.01$, $^{\#\#\#}p < 0.001$ compared with Control or AAV-*NC*+Veh group by student's t test and two-way ANOVA with Bonferroni post hoc test. $^{*}p < 0.05$, $^{**}p < 0.01$, $^{***}p < 0.001$ compared with PTX or AAV-*NC*+PTX group by One-way ANOVA with Dunnett's post-hoc test and two-way ANOVA with Bonferroni post hoc test. $F_{(10, 162)} = 4.02$ **(C)**, $F_{(10, 162)} = 8.59$ **(D)**, $F_{(10, 162)} = 7.27$ **(E)**, $F_{(16, 297)} = 3.16$ **(F)**, $F_{(16, 297)} = 5.51$ **(G)**, $F_{(16, 297)} = 2.98$ **(H)**, $F_{(2, 15)} = 13.2$ **(J)**.

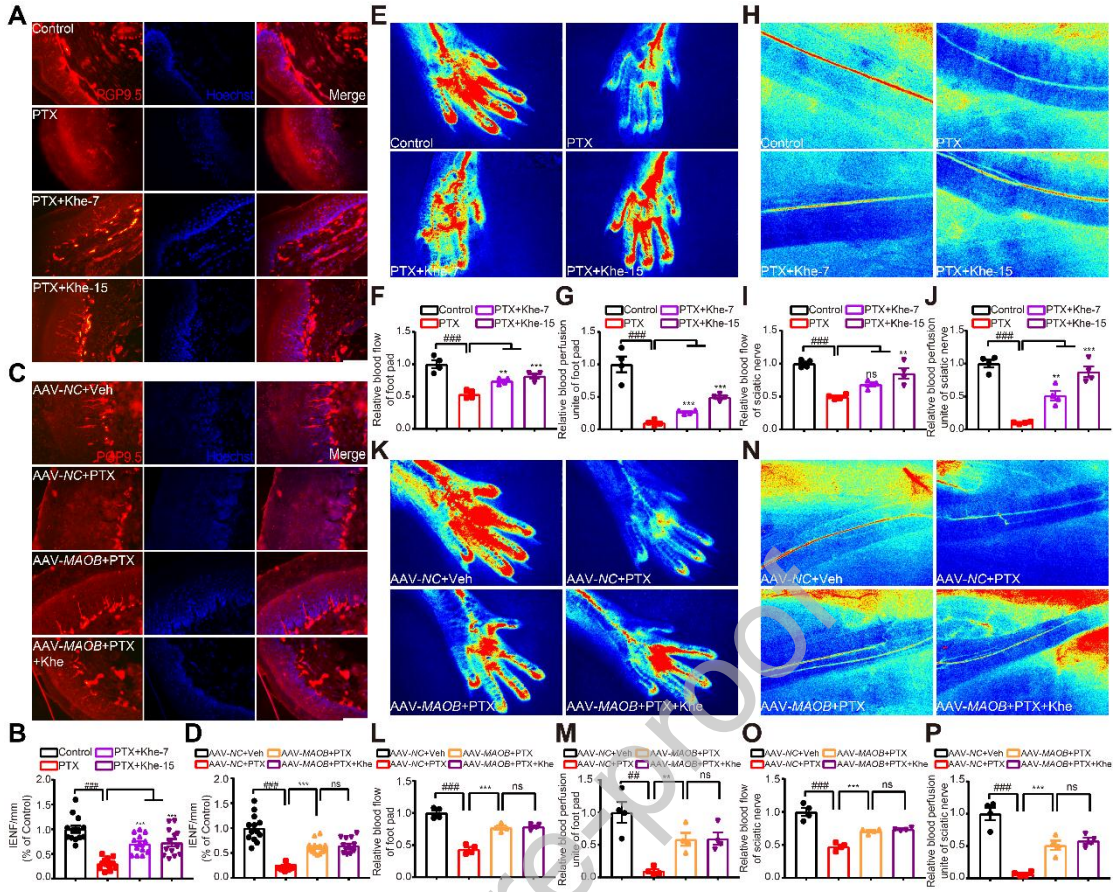

Fig. 6 Khe treatment improved peripheral nerve structure and vascular function in PIPN mice by targeting MAOB. Immunofluorescence (PGP 9.5 labelled IENF, red) with quantification results indicated that **(A, B)** Khe (7, 15 mg/kg/day) treatment or **(C, D)** AAV-*MAOB-shRNA* injection inhibited the PTX-induced IENF loss in foot pads of PIPN mice, and **(C, D)** Khe (15 mg/kg/day) treatment had no impacts on IENF density in foot pads of AAV-*MAOB-shRNA* injected PIPN mice (n = 13). Scale bar: 25 μm. Representative images with quantification results showed that **(E-J)** Khe (7, 15 mg/kg/day) treatment or **(K-P)** AAV-*MAOB-shRNA* injection increased the blood flow velocity and blood perfusion area in **(E-G, K-M)** foot pads and **(H-J, N-P)** sciatic nerve of PIPN mice, and Khe (15 mg/kg/day) treatment had no impacts on blood flow velocity and blood perfusion area in **(K-M)** foot pads and **(N-P)** sciatic

nerve of AAV-*MAOB-shRNA* injected PIPN mice (n = 4). Flow velocity and perfusion areas were shown as different colors as blue, green, yellow, orange, and red represented from low to high. All values were presented as mean ± SEM. $^{\#}p < 0.05$, $^{\#\#}p < 0.01$, $^{\#\#\#}p < 0.001$ compared with Control or AAV-*NC*+Veh group by student's t test. $^{*}p < 0.05$, $^{**}p < 0.01$, $^{***}p < 0.001$ compared with PTX or AAV-*NC*+PTX group by One-way ANOVA with Dunnett's post-hoc test. $F_{(2, 36)} = 18.3$ **(B)**, $F_{(2, 9)} = 22.64$ **(F)**, $F_{(2, 9)} = 2.241$ **(G)**, $F_{(2, 9)} = 82.14$ **(I)**, $F_{(2, 9)} = 16.75$ **(J)**.

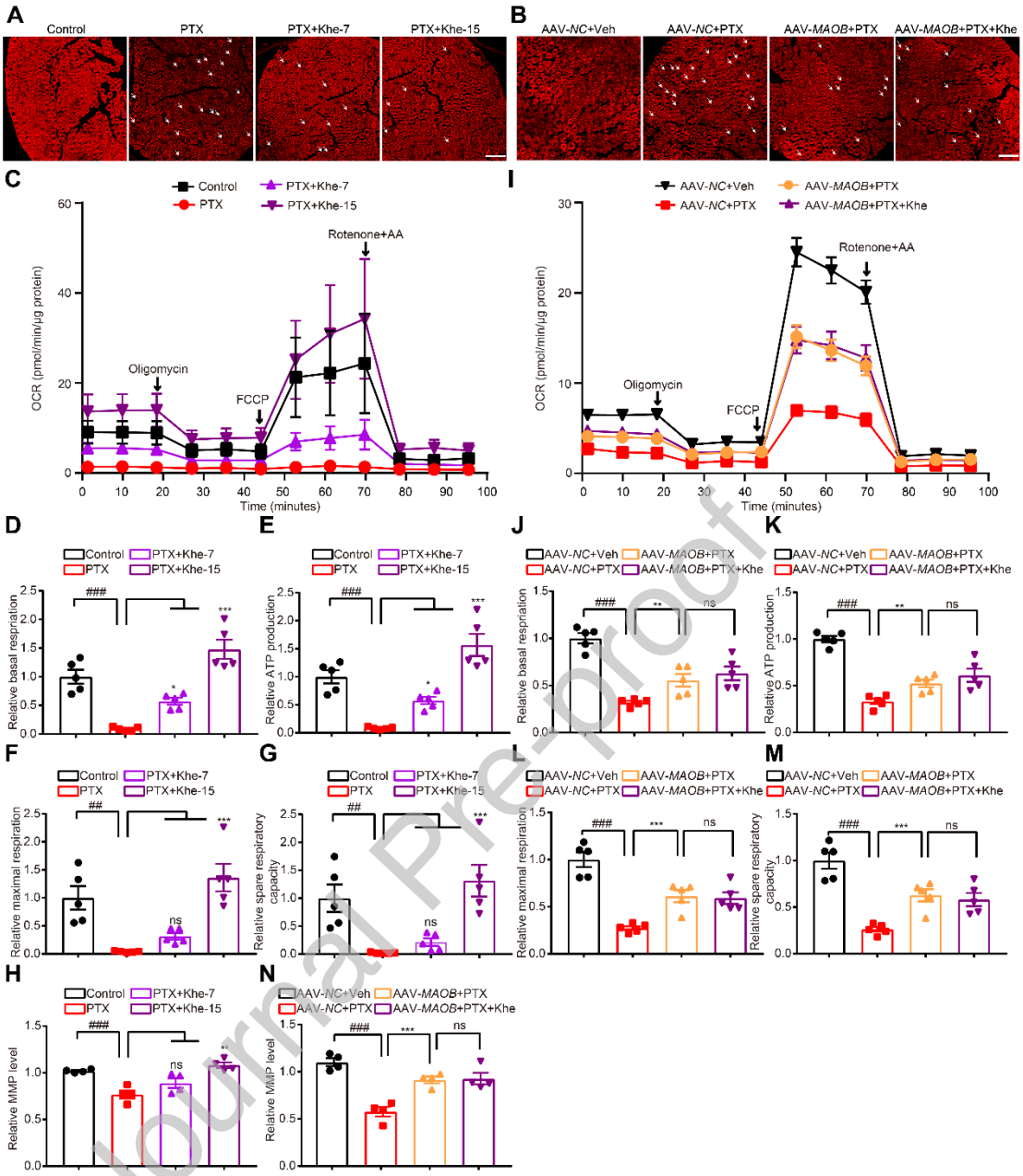

Fig. 7 Khe protected DRG neurons from demyelination and mitochondrial dysfunction in PIPN mice by targeting MAOB. Immunofluorescence (MBP labelled myelin basic protein, red) results showed that **(A)** Khe (7, 15 mg/kg/day) treatment or **(B)** AAV-*MAOB-shRNA* injection suppressed demyelination (arrows) and increased myelin sheath thickness of sciatic nerve in PIPN mice, and **(B)** Khe (15 mg/kg/day) had no impacts on myelin sheath structure in AAV-*MAOB-shRNA* injected

PIPN mice (n = 3). Scale bar: 25 μm. **(C, I)** OCR was measured at basal level with sequential addition of oligomycin (1 μM), FCCP (1 μM) and rotenone (1 μM) with antimycin A (1 μM) to DRG neurons from each group of mice (n = 5) using Xfe 24 analyzer. Khe (7, 15 mg/kg/day) treatment or AAV-*MAOB-shRNA* injection enhanced **(D, J)** basal respiration, **(E, K)** ATP production, **(F, L)** maximal respiration and **(G, M)** spare respiratory capacity in DRG neurons of PIPN mice (n = 5), and Khe (15 mg/kg/day) had no impacts on **(I)** OCR, **(J)** basal respiration, **(K)** ATP production, **(L)** maximal respiration and **(M)** spare respiratory capacity in DRG neurons of AAV-*MAOB-shRNA* injected PIPN mice (n = 5). **(H)** Khe (7, 15 mg/kg/day) treatment or **(N)** AAV-*MAOB-shRNA* injection upregulated the MMP level in DRG neurons of PIPN mice, and **(N)** Khe (15 mg/kg/day) had no impacts on MMP level in DRG neurons of AAV-*MAOB-shRNA* injected PIPN mice (n = 4). All values were presented as mean ± SEM. $^{\#}p < 0.05$, $^{\#\#}p < 0.01$, $^{\#\#\#}p < 0.001$ compared with Control or AAV-*NC*+Veh group by student's t test. $^{*}p < 0.05$, $^{**}p < 0.01$, $^{***}p < 0.001$ compared with PTX or AAV-*NC*+PTX group by One-way ANOVA with Dunnett's post-hoc test. $F_{(2, 12)} = 46.7$ **(D)**, $F_{(2, 12)} = 39.3$ **(E)**, $F_{(2, 12)} = 23.0$ **(F)**, $F_{(2, 12)} = 17.0$ **(G)**, $F_{(2, 9)} = 13.4$ **(H)**.

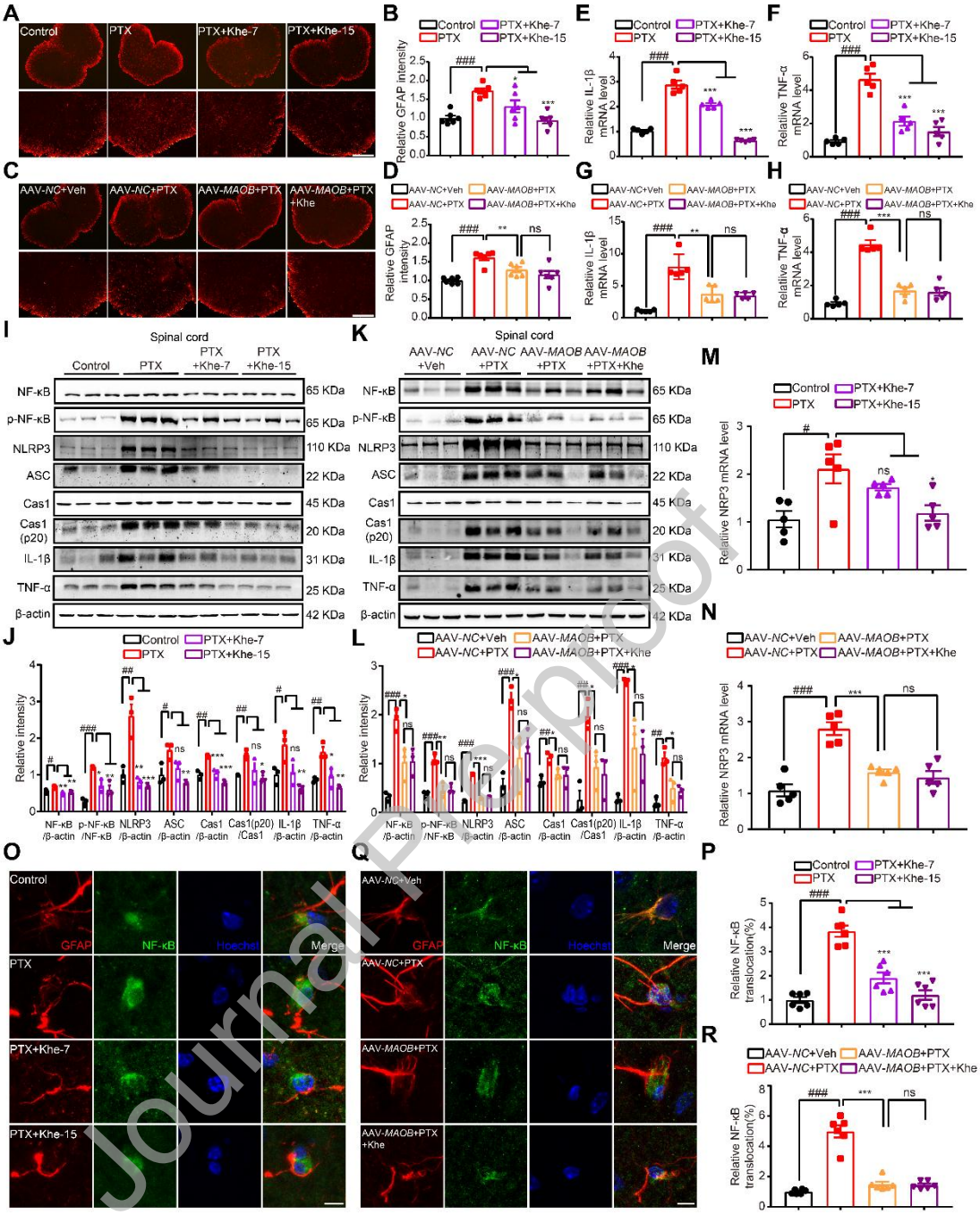

Fig.8 Khe treatment suppressed neuroinflammation of spinal cord in PIPN mice via MAOB/NF-κB/NLRP3/ASC/Caspase1/IL-1β pathway. Immunofluorescence (GFAP labelled astrocytes, red) with its quantification results demonstrated that **(A, B)** Khe (7, 15 mg/kg/day) treatment or **(C, D)** AAV-*MAOB-shRNA* injection inhibited SCDH astrocytes activation in PIPN mice, and **(C, D)** Khe (15 mg/kg/day) treatment had no such impacts in AAV-*MAOB-shRNA* injected PIPN mice (n = 6). Scale bar:

250, 100 μm. qRT-PCR results indicated that Khe (7, 15 mg/kg/day) treatment or AAV-*MAOB-shRNA* injection antagonized the mRNA levels of **(E, G)** IL-1β and **(F, H)** TNF-α in spinal cord of PIPN mice, and **(G, H)** Khe (15 mg/kg/day) treatment had no such impacts in spinal cord of AAV-*MAOB-shRNA* injected PIPN mice (n = 5). Western blot with its quantification results demonstrated that **(I, J)** Khe (7, 15 mg/kg/day) treatment or **(K, L)** AAV-*MAOB-shRNA* injection downregulated the protein levels of NF-κB, p-NF-κB, NLRP3, ASC, Caspase1, Cas1 (p20), IL-1β and TNF-α in spinal cord of PIPN mice, and **(K, L)** Khe (15 mg/kg/day) treatment had no such impacts in spinal cord of AAV-*MAOB-shRNA* injected PIPN mice (n = 3). qRT-PCR results indicated that Khe (7, 15 mg/kg/day) treatment or AAV-*MAOB-shRNA* injection antagonized the mRNA levels of **(M, N)** NLRP3 in spinal cord of PIPN mice, and **(**N**)** Khe (15 mg/kg/day) treatment had no such impact in spinal cord of AAV-*MAOB-shRNA* injected PIPN mice (n = 5). Immunofluorescence with quantification results demonstrated that **(O, P)** Khe (7, 15 mg/kg/day) treatment or **(Q, R)** AAV-*MAOB-shRNA* injection inhibited NF-κB nuclear translocation in SCDH astrocytes of PIPN mice, and **(Q, R)** Khe (15 mg/kg/day) treatment had no such effects in AAV-*MAOB-shRNA* injected PIPN mice (n = 6). Scale bar: 5 μm. β-actin was used as loading control in western blot assays. All values were presented as mean ± SEM. $^{\#}p < 0.05$, $^{\#\#}p < 0.01$, $^{\#\#\#}p < 0.001$ compared with Control or AAV-*NC*+Veh group by student's t test. $^{*}p < 0.05$, $^{**}p < 0.01$, $^{***}p < 0.001$ compared with PTX or AAV-*NC*+PTX group by One-way ANOVA with Dunnett's post-hoc test. $F_{(2, 15)} = 12.65$ **(B)**, $F_{(2, 12)} = 128$ **(E)**, $F_{(2, 12)} = 31.4$ **(F)**,

$F_{(2, 6)}$ = 19.9 for NF-κB **(J)**, $F_{(2, 6)}$ = 11.7 for p-NF-κB **(J)**, $F_{(2, 6)}$ = 32.5 for NLRP3 **(J)**, $F_{(2, 6)}$ = 13.2 for ASC **(J)**, $F_{(2, 6)}$ = 58.2 for Cas1 **(J)**, $F_{(2, 6)}$ = 6.82 for Cas1 (p20) **(J)**, $F_{(2, 6)}$ = 10.5 for IL-1β **(J)**, $F_{(2, 6)}$ = 17.3 for TNF-α **(J)**, $F_{(2, 12)}$ = 5.24 **(M)**, $F_{(2, 15)}$ = 38.58 **(P)**.

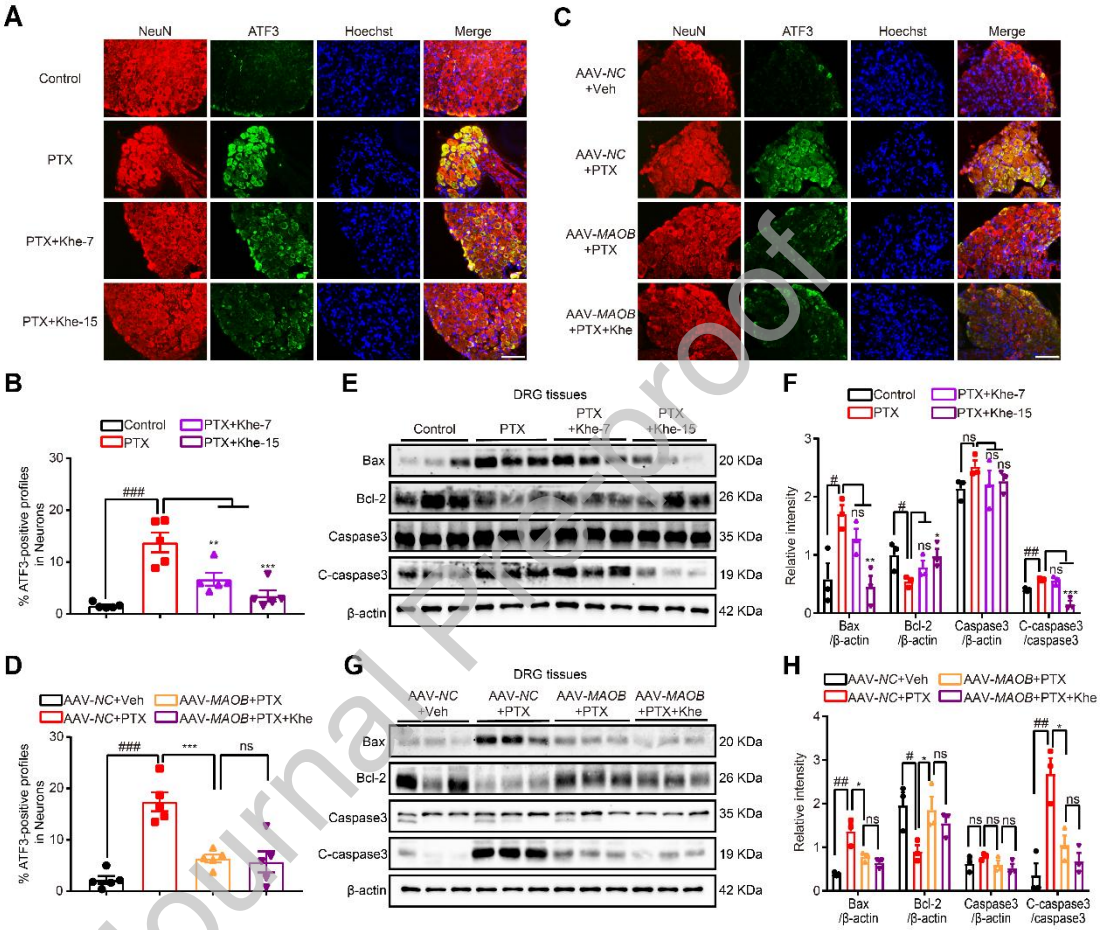

Fig. 9 Khe treatment protected against DRG neuronal damage or apoptosis in PIPN mice by targeting MAOB. Immunofluorescence with its quantification results demonstrated that **(A, B)** Khe (7, 15 mg/kg/day) treatment or **(C, D)** AAV-*MAOB-shRNA* injection repressed ATF3 number in DRG neurons of PIPN mice, and **(C, D)** Khe (15 mg/kg/day) treatment had no impacts on neuronal damage in DRG neurons of AAV-*MAOB-shRNA* injected PIPN mice (n = 5). Scale bar: 25 μm. Western blot with quantification results indicated that **(E, F)** Khe (7, 15 mg/kg/day)

treatment or **(G, H)** AAV-MAOB-shRNA injection upregulated the expression of anti-apoptotic protein Bcl-2 and downregulated the expressions of pro-apoptotic protein Bax and C-caspase3 in DRG tissues of PIPN mice, and **(G, H)** Khe (15 mg/kg/day) had no impacts on apoptotic-associated proteins in DRG tissues of AAV-*MAOB-shRNA* injected PIPN mice (n = 3). β-actin was used as loading control in western blot assays. All values were presented as mean ± SEM. $^{\#}p < 0.05$, $^{\#\#}p < 0.01$, $^{\#\#\#}p < 0.001$ compared with Control or AAV-*NC*+Veh group by student's t test. $^{*}p < 0.05$, $^{**}p < 0.01$, $^{***}p < 0.001$ compared with PTX or AAV-*NC*+PTX group by One-way ANOVA with Dunnett's post-hoc test. $F_{(2, 12)} = 13.2$ **(B)**, $F_{(2, 6)} = 14.2$ for Bax **(F)**, $F_{(2, 6)} = 4.51$ for Bcl-2 **(F)**, $F_{(2, 6)} = 0.9616$ for Caspase3 **(F)**, $F_{(2, 6)} = 33.0$ for C-caspase3 **(F)**.

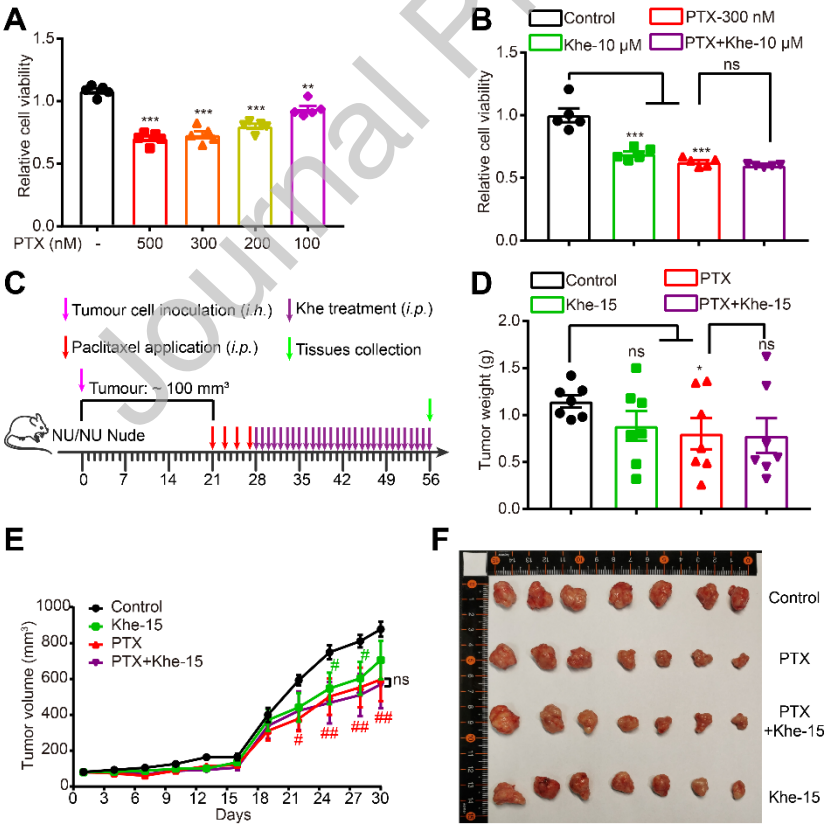

Fig. 10 Khe had no effects on the antitumor activity of PTX. **(A)** MTT assay

results demonstrated that PTX reduced the cell viability of MCF7 cells at concentrations of 100, 200, 300 and 500 nM (n = 5). **(B)** MTT assay results demonstrated that Khe (10 μM) had no effect on the antitumor activity of PTX (300 nM) *in vitro* (n = 5). **(C)** Schedule showing the treatment regimen used in a tumor xenograft model of human breast cancer. Quantitative results of **(D)** tumor weight and **(E)** tumor volume after subcutaneous inoculation with MCF 7 cells. **(F)** Photograph of autopsies performed at the end of the experiment in each group. All values were presented as mean ± SEM. $^{*}p < 0.05$, $^{**}p < 0.01$, $^{***}p < 0.001$ compared with DMSO group by Student's t test. $^{\#}p < 0.05$, $^{\#\#}p < 0.01$, $^{\#\#\#}p < 0.001$ compared with Control group by One-way ANOVA with Dunnett's post-hoc test. $F_{(10, 132)} = 0.0716$ **(E)**.

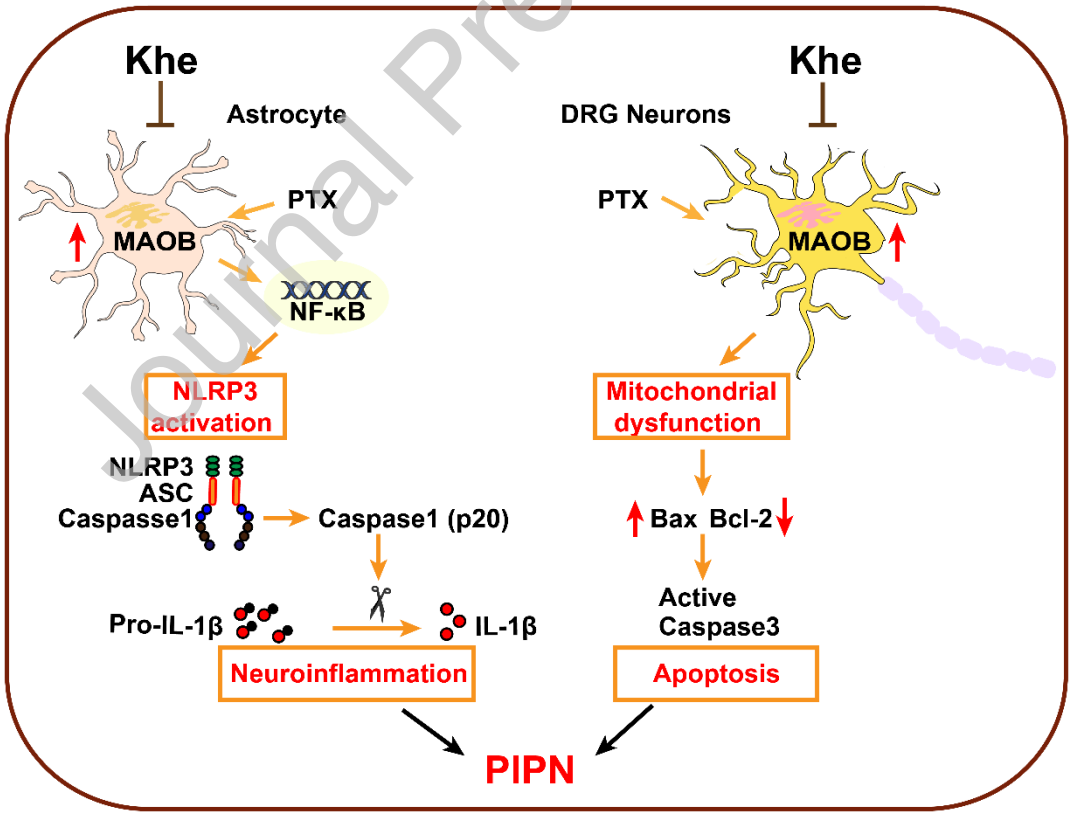

Fig.11 Khe as a selective MAOB inhibitor ameliorated paclitaxel-induced

peripheral neuropathy in mice. Khe improved mitochondrial dysfunction of DRG neurons and further alleviated apoptosis by regulation of apoptosis-related protein such as Bcl-2, Bax and C-caspase3 in PIPN mice by targeting MAOB. In addition, Khe also inhibited spinal astrocytes activation and suppressed neuroinflammation of spinal astrocytes in PIPN mice via MAOB/NF-κB/NLRP3/ASC/Caspase1/IL-1β pathway.